SYNTHESIS AND CHARACTERIZATION OF CARBON NANOFILMS FOR CHEMICAL SENSING

by

Vivek Kumar, MS

A dissertation submitted to the Graduate Faculty in Chemistry in partial fulfillment of the requirements for the degree of Doctor of Philosophy, The City University of New York

2012

This manuscript has been read and accepted for the Graduate Faculty in Chemistry in satisfaction of the dissertation requirement for the degree of Doctor of Philosophy.

Prof. Alexander M. Zaitsev

Date

Chair of Examining Committee

Prof. Maria Tamargo

Date

Executive Officer

Prof. Louis J. Massa

Prof. Yasha Yi

Supervisory Committee

THE CITY UNIVERSITY OF NEW YORK

Abstract

SYNTHESIS AND CHARACTERIZATION OF CARBON NANOFILMS FOR CHEMICAL SENSING

by

Vivek Kumar

Adviser: Prof. Alexander M. Zaitsev

Carbon nanofilms obtained by high temperature graphitization of diamond surface in inert atmospheres or vacuum are modified by treatment in plasma of different precursor gases. At temperatures above 1000 ^{o}C, a stable conductive film of thickness between 10 – 100 nm and specific resistivity 10^{-3}–10^{-4} Ω.m, depending upon the heating conditions and the growth atmosphere, is formed on diamond surface. A gray, thin film of high surface resistivity is obtained in high vacuum, while at low vacuum (below 10^{-4} mbar), a thick black film of low surface resistivity forms. It is observed that the exposure to plasma reduces the surface conductance of carbon nanofilms as result of a partial removal of carbon and the plasma-stimulated amorphization. The rate of the reduction of conductance and hence the etching ability of plasma depends on the type of precursor gas. Hydrogen reveals the strongest etching ability, followed by oxygen and argon, whereas SF_6 is ineffective. The carbon nanofilms show significant sensitivity of their electrical conductance to temperature and exposure to the vapors of common organic compounds. The oxygen plasma treated films exhibit selective response to acetone and water vapors. The fast response and recovery of the conductance are the features of the carbon nanofilms. The plasma-treated carbon nanofilm on graphitized diamond surface is discussed as a promising sensing material for development of

all-carbon chemical sensors, which may be suitable for biological and medical applications.

An alternative approach of fabrication of temperature and chemical sensitive carbon nanofilms on insulating substrates is proposed. The films are obtained by direct deposition of sputtered carbon on highly polished quartz substrates followed by subsequent annealing at temperatures above 400 ^{o}C. It is observed that the as-deposited films are essentially amorphous, while the heating induces irreversible structural ordering and gradual conversion of amorphous carbon in disordered graphite. This evolution is confirmed by Raman spectroscopy and electrical measurements.

The carbon nanofilms grown on diamond and deposited on quartz both show similar exponential dependence of their conductance on temperature, which is essentially different from the usual behavior of the thermally activated conduction and the conduction due to variable range hopping of charge carriers. The observed exponential dependence of conductance is explained by a model based on the thermally vibrating energy barriers.

The as-grown nanofilms on diamond surface show a negative response (decrease in conductance) to the vapors of acetone, toluene and hexane, and a positive response (increase in conductance) to the water vapor. Sensitivity (relative change in conductance) to toluene is greater than to water, acetone, and hexane, in that order. Plasma exposure alters the sensitivity to positive for all the organic vapors. Overall, an increase in sensitivity is observed with the plasma exposure time. For acetone and water, an increased exponential dependence on vapor concentration is also observed. The exposure to oxygen plasma renders the carbon films on diamond selectively sensitive to acetone and water vapors. The hydrogen plasma exposure makes the films selectively sensitive to toluene vapor. It is found that the carbon nanofilms on quartz have p-type conductivity, as indicated by the opposite response to NO_2 and NH_3 analytes. NO_2, a known electron acceptor, increases the conductance. NH_3, a known electron donor, decreases the conductance. The phenomenological description of the chemical

sensitivity of the carbon nanofilms $\sigma = \beta/\tau$ is proposed as a function of two main parameters: the time constant τ and the maximum relative change in conductance β. τ and β are described as the parameters related to the surface and bulk material properties of the films, respectively.

Dedicated to

My Grandparents

Mrs. Shanti Devi and the late Saryu Prasad Suman
The late Rajmati Devi and Shivnath Prasad

and

My Parents

Mrs. Savita Suman and Mr. Brajkishore Prasad

Acknowledgements

First and foremost, I would like to express my deepest gratitude to my adviser, Prof. Alexander M. Zaitsev, for his encouragement, guidance, and support during my doctoral research. He has been a constant source of inspiration, both professionally and personally. I am fortunate to work under his mentorship which helped me grow as a scientist and an independent thinker.

My sincere gratitude to the members of my doctoral committee, Prof. Louis J. Massa and Prof. Yasha Yi, for generously giving of their time and expertise to better my work. I greatly value the guidance and support they provided for my professional growth.

I would also like to take this opportunity to acknowledge the financial and academic support of the City University of New York and the College of Staten Island. Also acknowledged are grants from the Army Research Office and PSC-CUNY. I am grateful to the members of the faculty for helpful suggestions during formal and informal interactions. In particular, I would like to thank Prof. Alan Lyons for his scientific insight and valuable suggestions for my research, and our campus lab safety supervisor, Mr. James Saccardo for his exemplary mentorship in lab safety and his spirited helpfulness. Thanks to Mr. Manik Mandal and other friends at CSI for their great company.

I owe so much to my grandparents, parents, wife, brother, sister and other family members; their purest love, endless support, and undying belief in my abilities mean everything to me. My lovely wife Priyanka provided unmatched care, comfort, and help during preparation of this dissertation. I wish to express my gratitude to my countrymen for motivation to excel in a far away land. Finally, obeisance to Maa Saraswati – the goddess of knowledge, for being the source of inner strength.

Table of contents

List of Figures

Chapter I

Introduction

1.1 Motivation

Sensors have widespread applications in industry and scientific research, and may be broadly categorized as physical or chemical, depending on the changes they sense [1-3]. Physical sensors sense changes in physical parameters, such as pressure or temperature [4], whereas chemical sensors detect the presence of molecules (or ions) in gas or solution phase [2, 3]. Though there are varieties of effective physical sensors available, realization of selective and practical chemical sensors is still an area of hot pursuit. This encourages the exploration of novel sensing materials and the design of sophisticated sensor structures for chemical sensing.

1.2 Objectives

The present work focuses on the utilization of carbon nanofilms as chemical sensing materials in solid state chemical sensors. The specific objectives of the research are: synthesis and characterization of carbon nanofilms on insulating substrates, study of thermally induced structural ordering in carbon nanofilms and its role in sensing properties, physical methods of modification of carbon films and control of their material structure for selective sensing, understanding of charge transport in less-ordered carbons, and elucidation of observed temperature and chemical sensitivity of conductance.

1.3 Scope and achievements of the research

Carbon is a potential electronic material for a number of applications. The principal ***scientific merit*** of the doctoral research is the study of the sensing properties of carbon nanofilms which also contributes to the understanding of their electronic properties. The broader scope or significance of the doctoral research is the design of selective chemical sensors with potential application in biomedical devices. In this regard, the graphite/diamond hybrid system holds promise as an all-carbon technology. There have not been systematic studies of such all-carbon devices, and the doctoral research attempts fabrication of rudimentary all-carbon temperature and chemical sensors and discusses their properties.

The main achievements of the doctoral research are: demonstration of a rudimentary all-carbon sensor for biomedical applications, ascertainment of the growth condition for high temperature graphitization of diamond by in-situ measurements, and determination of the role of plasma in selective chemical sensing. A model for charge transport in low-ordered carbon films that successfully explains the mechanism for temperature and chemical sensing is also proposed. The research resulted into two articles in a peer-reviewed journal [5, 6], and presentations in several international conferences. A provisional patent [7] has also been filed on carbon nanofilm sensors. A summary of the major results of the research is provided in a separate section at the end of the last chapter.

1.5 Organization of the dissertation

The dissertation is organized into four chapters. The first chapter is on background of the research, the second chapter describes the experimental design and methodologies adopted, and the last two chapters discuss the experimental results. The results on carbon nanofilms on diamond for all-carbon sensor applications are discussed in the third chapter, and include in situ study of graphitization of diamond, surface characterization by atomic force microscopy and Raman spectroscopy, and plasma modification of carbon films in different precursor gases and its effect on temperature and chemical sensing. The fourth chapter which presents the results on carbon nanofilms on quartz describes the thermally induced structural ordering in an amorphous carbon film and effect on the temperature and chemical sensing properties. Also proposed are the model for electrical conductance in low-ordered carbon nanofilms, and the mechanism for chemical sensing. In a separate section at the end of the fourth chapter, a summary of the important results of the research is provided.

1.6 Background of the research

The chemical sensor research is an interdisciplinary area, attracting scientists and engineers alike [3, 8]. The realization of an effective chemical sensor involves many stages from material design to device integration. The complexity of the issue becomes even bigger with many chemical species of interest. This makes a complete review of the field difficult. Nevertheless, the dissertation presents an overview of the state of the art that pertains to the use of carbon materials for sensing and also sets the direction for the doctoral research. After a description of the common sensor characteristics and type, an overview of the other sensing materials followed by a more detailed review of the carbon materials is presented.

1.6.1 Sensor characteristics

The main characteristics of chemical sensors are: sensitivity, response time, recovery time, selectivity, operating temperature, reproducibility, and stability [3, 8]. Additional characteristics that need consideration include: size, practicality and cost.

Sensitivity: The usual definition of sensitivity is given in terms of the ratio of the measured sensitive property on exposure (P_e) and when in an inert gas (P_i), given by the expression: P_e/P_i., or the relative % change: $\Delta P/P_i$ x 100. At times, air is also used as a reference if there is no significant sensitivity or interference by air. An alternate method to describe sensitivity using two separate parameters is introduced in the chapter 4.

Response time: Response time is usually defined as the time required by sensor to attain a certain % of the maximum observed sensitivity, usually 90%, or the saturation.

Recovery time: Sensor may take unreasonably long to recover to its original condition and it's important to define a limit which prepares the sensor to respond reproducibly in the next exposure. Usually, this limit is set within few % of the initial value of the sensitive property and the time to reach the limit is called as recovery time.

Selectivity: The selectivity is given in terms of the sensitivity coefficient: the ratio of sensitivities for analyte and interfering compound. Often, cross-sensitivity curves are obtained to determine selectivity.

Operating temperature: Operating temperature of a sensor is the temperature at which the sensitivity of the sensor is maximum, and decides its suitability for a particular application. Chemical sensors working at room temperature are more in demand, and high operating temperature-sensors are needed for operations at elevated temperatures [9]. However, stability of sensor at high temperature is a critical consideration in sensor design.

Reproducibility and stability: Both concern the reliability of the sensor. In the absence

of a definite method of quantification, usually a comparison of sensor performance over a certain interval of time and/or number of exposure is conducted.

An ideal sensor should excel in all the above parameters with the existing gap setting the directions for the future research, and have been discussed in more detail within the scope of the present work.

1.6.2 Sensor types and designs

Sensing property, sensing material, sensor architecture, and working principle - all may be used to classify sensor type. As mentioned in the opening paragraph, based on sensing property sensors may be broadly classified as: physical and chemical. Further, a physical sensor could be a pressure sensor, temperature sensor, strain sensor, and so on; whereas, a chemical sensor could be an ion sensor, gas/vapor sensor, and biosensor. In this regard, branching out of biosensors as a separate field is noteworthy [10-17]. For gas/vapor sensing (henceforth, referred as chemical sensing, unless otherwise specified), which is the focus of the present study, the main sensing materials are: metal-oxide [18-20], polymers [21-29], carbon nanotubes (CNTs) [30-34], and their hybrids [26, 35-39]. With regard to sensor architecture and working principle, there are numerous different approaches and hence sensor types. For our interest in carbon based solid state chemical sensors we have briefly reviewed some of the sensor architectures and underlying working principles that have already shown potential.

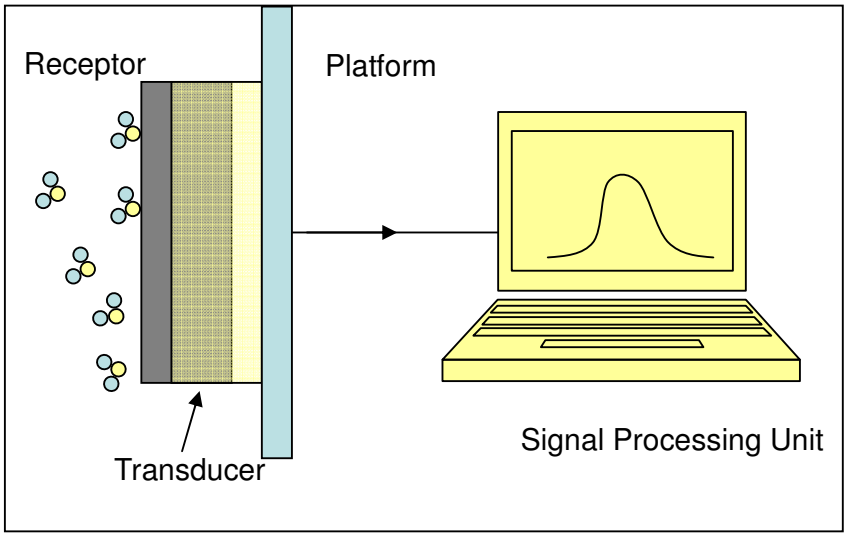

Fig. 1.1. Basic architecture of a chemical sensor.

Basic architecture of a sensor consists of a receptor integrated with a transducer (Fig. 1). The sensing device is connected to a signal processing unit, usually a computer with an appropriate data collection interface. The receptor which interacts physically and/or chemically with chemical analytes causes a modulation in the properties of the transducer, usually electronic. At times, receptor and transducer are indistinguishable and refereed together as sensing material. For example, in a resistor sensor, interaction at the surface causes change in the resistance of the same material and is recorded as response [5, 40]. In comparison, in a surface acoustic wave (SAW) sensor [41, 42], the molecular adsorption on the sensitive coating (receptor) on a piezoelectric surface (transducer) causes modulation in the piezoelectric current generated by the surface acoustic waves, and recorded as sensor response.

Fig. 2 and Fig. 3 illustrate the schematic designs of common sensor types. The resistor sensor (A), the simplest of all sensor types, is based on the modulation of resistance/conductance. Usually, a semiconducting material is employed as the sensing material, and the significant resistance changes occur on charge transfers with a reducing or

oxidizing gas. The field effect transistor (FET) sensors (B) [43, 44]are the most effective sensors which utilize change in electronic properties of the sensing material in the gate, and the response is observed in the drain current, I_D. Electrochemical sensor (C) [15, 45] consists of a sensing electrode, and a counter electrode separated by an electrolyte medium. Working in amperometric mode, current proportional to the gas concentration is produced across the electrodes, and recorded as the sensor response. Most of the commercially employed gas sensors, for example, carbon monoxide sensors, are electrochemical. Ionization senor (D) [46-52] relies on the dissociation of gas molecules at the high electric field generated at the sharp tips of its electrodes. In this regard, CNTs having nanometer sized tips and high tensile strength, showed great potential. SAW sensor (E) [41, 42] utilizes the mass changes due to the adsorbed molecules on the sensing layer to modulate the piezoelectric current in the substrate below. SAWs are generated by the two interdigitated wave transducer electrodes.

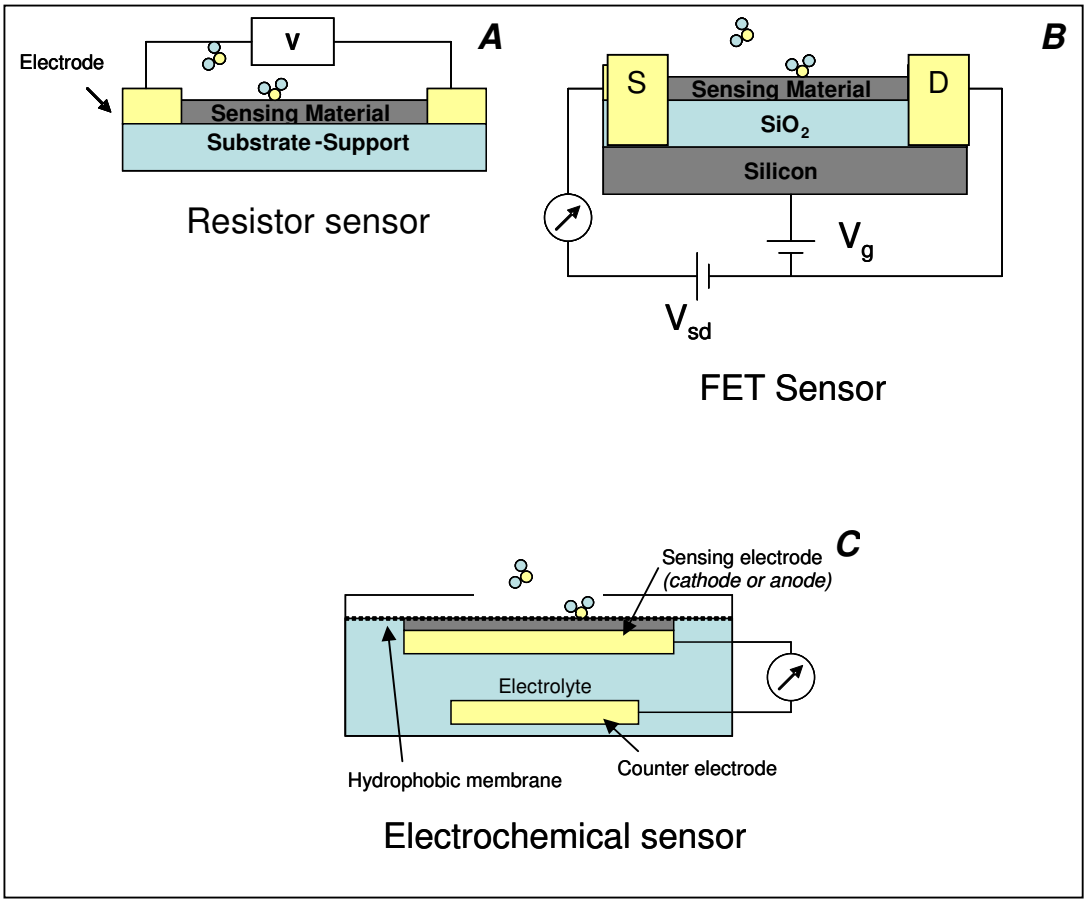

Fig. 1.2. Common sensor types: Resistor (A), FET (B) and Electrochemical (C).

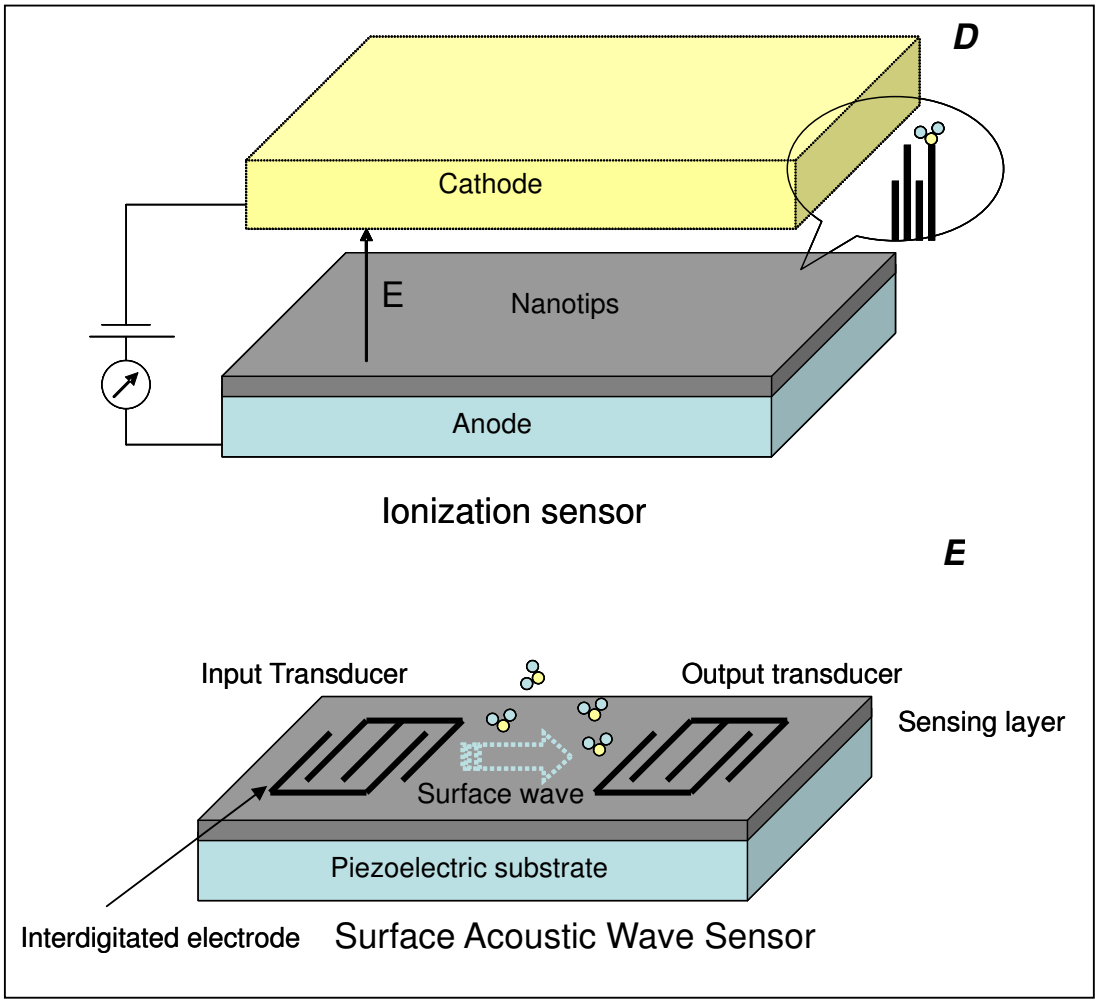

Fig. 1.3. Common sensor types, contd.: Ionization (D), Surface Acoustic Wave (E).

1.6.3 Overview of present technology

Recent developments in nanotechnology have helped considerably in fabricating effective chemical sensors. Mainly, metal-oxides[18], conducting polymers [21-25, 27-29], carbon nanotubes (CNTs) [15, 30, 34] and their composites [26, 36, 37, 39] have been tried for chemical sensing applications. Metal-oxide based sensors have been known for a long time. They are particularly successful in detecting different gases/vapors at a sub-ppm concentration with reasonable stability. However, their high operating temperature (over 300°C) poses a serious restriction on their employability. In contrast, the sensors, which are based on conducting polymers and carbon nanotubes, work at room temperature. They also provide additional benefit of modification of the active material to help to achieve chemical selectivity. The main drawback with the use of conducting polymers is their low response and low stability. Concerning carbon nanotubes, their ability to detect sub-ppm concentrations of gases is remarkable. However, the recovery time of the carbon nanotube based sensors has been found to be very long (~10 hours) and, in order to reduce this time, special procedures (e.g. ultraviolet light illumination) are required [32]. CNTs and other carbon materials are discussed further.

1.6.4 Carbon sensors

The renewed interest in carbon as an electronic material was triggered by the discovery of its atomically highly ordered forms like fullerenes [53], carbon nanotubes (CNTs) [54], and graphenes and their interesting electronic properties [55, 56]. The growing environmental concern has also served as a motivation, as carbon is considered to be bio-

compatible. Newer applications are being explored with these nanostructured carbons along with traditionally known bulk forms of carbon, diamond and graphite. Less ordered forms like amorphous carbons have not received similar attention due to their inferior electronic properties. However, more useful applications may be expected through control of their material order giving insulating to conductive carbons [57-59]. An important advantage is their relatively easy preparation by a number of different methods.

Chemical sensing is one such area—important for both industry and research— where carbon materials are studied. Graphenes [60, 61] and CNTs [15, 30, 31, 33, 34, 40] have already shown potential as sensing material with remarkable sensitivities in their conductance to ppm level concentrations of vapors of some common analytes. Also, unlike commercially employed metal-oxide-based sensors they do not need high operating temperatures and can work at room temperature as well. These results encourage study of carbon films especially those with significant graphitic content.

1.6.4 Chemical sensors based on carbon nanotubes

In two decades since their discovery[54], carbon nanotubes (CNTs) along with graphenes have established themselves among the most promising electronic materials for a variety of applications[10, 30, 34, 62-68]. The focus of the active research is into the areas concerned with, synthesis, characterization, properties, modification, device fabrication and application. The report briefly reviews the progress made which also concerns sensor based applications.

a. Properties

The quasi one dimensional structure of CNTs and SP^2 bonding network give CNTs interesting electronic[56] and mechanical properties[69], which further depend on their

geometry (diameter, chirality), number of layers and structure of the aggregates they are present in. The metallic to semiconducting characteristics of SWNTs depending on geometry, and the ballistic transport in CNTs are their most useful electronic properties. The superior mechanical properties include high tensile strength and elasticity. These properties when combined with their small dimensions and large surface area make CNTs promising for developing miniature electronic devices, including those for chemical sensing. Further, the increased adsorption of gas molecules in the gaps between nanotubes walls gives them an edge over graphene based gas sensors.

b. Synthesis

The current methods of synthesis of CNTs are based on one of the three techniques[70-72]: carbon arc-discharge[73-75], laser ablation[76, 77], and chemical vapor deposition (CVD)[78]. In carbon arc-discharge method, the CNTs are formed by arc discharge between two carbon electrodes. While MWNTs do not need any catalysts, SWNTs form in the presence of catalysts like Co and Ni. The laser-ablation technique involves use of laser pulses to ablate a carbon target in the presence of an inert gas. The ablated carbons form CNTs and suitable catalysts are required to selectively obtain SWNTs. In CVD technique, sufficient energy is supplied to a hydrocarbon gas usually methane or acetylene to cleave its molecules into radicals, in the presence of a catalyst supported over a substrate. The energy may be supplied either by direct heating or microwave application. In a modification of the process, known as radio frequency plasma-enhanced CVD (RF PECVD), plasma of the precursor gas is generated using radio frequency prior to the CVD process.

The final product which is generally a mixture of different types of CNTs is also accompanied by other carbonaceous materials as impurity. The post production purification involves oxidation of the impurities by common oxidizing agents such as sulfuric acid, nitric

acid, or $KMnO_4$. However, the accompanied damage to the CNTs is unavoidable. The main research efforts are directed toward economical method for large-scale production of high purity CNTs of a specific type.

c. Application as sensing material

Different kinds of CNT chemical sensors with ppm level sensitivity, fast response, reversibility, and reasonable stability have been demonstrated [14-17, 30, 31, 33, 34, 40-42, 79-94]. Though, semiconducting SWNTs are more useful for the large sensitivity of their electronic properties, MWNTs are also being studied for their easier preparation. As mentioned before, the increased adsorption of gas molecules in the gaps between nanotubes walls gives them an edge over graphene based gas sensors. Further, the advancement in functionalization methods for CNTs makes them immensely promising as chemical sensing materials[95-97]. Like any other technology, limitations exist, and are discussed in the last part of this section.

Conduction: First reported by Kong et al [40], modulation of conductance of CNTs on exposure to oxidizing and reducing gases has been widely investigated. The gases so studied include: H_2, NH_3, NO_2, CH_3OH and O_2. The behavior is attributed to p-type character of semiconducting CNTs, wherein the charge density is affected on interaction with analyte molecules. The sensors hence made, outsmart those based on semiconductor oxides, for their significantly higher sensitivity and faster response even at room temperature. For example, the sensor made by Kong et al, showed an increase in resistance of the order of about 3 orders of magnitude on exposure to ppm level concentration of NO_2 and NH_3 in just about 2-3 seconds.

The functionalization of MWNTs with Pd and Pt was used to obtained hydrogen sensitive thin films [98], whose resistance increased upon exposure to hydrogen. Though, the

similar response was observed for other reducing gases like NH_3 and CH_4, the sensitivity to hydrogen was much higher. The high and selective sensitivity for H_2 along with reversibility and stability even after multiple exposure cycles showed a potential for making practical hydrogen sensors. In another report by Valentini et al, thin films of CNT grown on Si_3N_4 was shown to have ppb level sensitivity to the common reducing and oxidizing gases [90, 99]. An increased sensitivity to NO_2, and a maximum response at 165 ^{0}C was observed on annealing the as grown films at temperatures higher than 330 ^{0}C .

Field-effect transistor: CNTs have also been utilized as active sensing material in a FET based sensor [100]. The performance of pristine CNTs in FET sensors has opened a wide scope for further functionalization to incorporate specific chemical recognition sites to enhance selectivity. In this regard, functionalization of CNTs with DNA or other biochemical molecules looks very attractive for making biosensors. In a pioneering study by Staii et al, single-stranded DNAs were immobilized on SWNTs to sense specific gases [101].

Electrochemical: CNTs functionalized with chemical recognition sites when grafted on the sensing electrodes, facilitate the electron transfer process between the electrodes and binding molecules. This has enabled development of electrochemical sensors with CNTs as integral part especially for the detection of biomolecules, which have low electrochemical reactivity. Such a biosensor was developed by Sotiropoulou and Chantiotakis for detection of glucose molecules [102]. The molecules of enzyme glucose oxidase, immobilized on the CNT arrays, oxidize the incoming glucose molecules, and the electrons are transferred to the electrode through CNT.

Capacitor: Capacitor sensors based on modulation of capacitance due to the dielectric changes in the CNT sensing material have also been reported. Suehiro et al constructed a sensor for ammonia showing positive sensitivity of capacitance. Later, in a pioneering work, SWNTs showed a high sensitivity of their capacitance to a broad class of chemical vapors.

The proposed mechanism was based on the polarization of molecular adsorbates by the fringing electric field at the surface. The main advantages of capacitor sensors are their lower power consumption and very fast recovery (few seconds).

Gas-Ionization: Gas ionization sensors utilizing CNTs as electrode have also been developed [46-52]. The high electric field at the sharp tips of CNTs caused dissociation of the gas molecules. Unlike conductance based CNTs, they were not limited by low adsorption.

Thermoelectric: The sensitivity of thermoelectric power across a CNT structure has been utilized for chemical sensing [103]. Interestingly, metallic CNTs show higher sensitivity.

Acoustic: SAW sensors utilize piezoelectric detection of the adsorbed molecules on CNTs [41]. CNTs are coated on a piezoelectric substrate in which acoustic waves are generated, and a modulation in its resonant frequency is recorded as the sensor response. Sensitivity of resonance frequency of CNTs coated on quartz was studied for many volatile organic compounds. The selectivity to different analytes was found to be dependent on the type of solvent used to disperse the CNTs during the coating process, thereby, suggesting a method for making selective chemical sensors.

d. Outlook

Ability to CNT sensors to detect sub-ppm concentrations of gases is remarkable. However, the recovery time of the carbon nanotube based sensors has been found to be very long (~10 hours) and, in order to reduce this time, special procedures (e.g. ultraviolet light illumination) are required [32]. It may also be noted that only single wall carbon nanotubes (SWNTs): individual [40] and thin films made of SWNTs [31, 80, 83]; perform reasonably well. Additionally, performance will depend upon type of SWNT, which may be metallic, or semiconducting depending on their geometry [55], with semiconducting SWNT showing greater response. Response from a SWNT film is averaged over different types of tubes

present and is hence lower. MWNTs show much lower response and have been tried as composites with metal oxides [104] and polymers [26, 35, 36, 38, 39]. Thus, technological hurdle imposed by the difficulty in obtaining pure SWNTs of desired geometry and the long recovery time are the challenges still to be met on the way of development of effective gas sensors based on carbon nanotubes. Another, major hurdle in the use of CNTs is the concern with their biocompatibility which needs to be thoroughly examined [13, 105-115].

1.6.6 Chemical sensors based on diamond

Diamond has been extensively utilized as a material of choice for biosensor application[12] for its chemical inertness and biocompatibility, along with its superior electronic[116] and mechanical properties that make it an ideal substrate for other electronic applications as well. Mostly employed as electrodes in biosensors, the other benefits come from low background current, large electrochemical window and the presence of a quasi-two-dimensional conductive layer[117] at the surface of hydrogen terminated diamond. In addition, once thought to be chemically inert, advancement in many modification techniques for diamond which include – chemical functionalization, plasma modification and bulk doping has opened up a plethora of opportunities in its utilization.

Though, major interest in diamond for sensing application is as electrodes in biochemical sensors and piezoresistive sensors, there have been some efforts to use them for gas sensing [9, 118-123]. In one of the earliest efforts, a microelectronic hydrogen gas sensor based on metal-insulator-semiconductor Schottky-diode configuration with palladium as metal, intrinsic polycrystalline diamond film (I-diamond) as insulator, and a boron doped p-type polycrystalline diamond film (p-diamond) as semiconductor was constructed by Kang et

al. [123] In another study, it was proposed that adsorbed hydrogen molecules on dissociation at the palladium surface diffused to the metal-insulator interface creating a dipole layer, thereby, changing the work function difference at the interface, and hence response of the device [9]. The same device was later reported to be sensitive to organic vapors: benzene and toluene [124], and when using tin oxide in place of oxygen made them sensitive to oxygen [121]. The sensitivity of these sensors was found to increase with temperature. The high thermal stability of diamond makes them particularly useful for high-temperature applications.

1.6.7 Chemical sensors based on diamond-like carbon (DLC)

DLCs are amorphous carbons with high fraction of sp^3 bonding [125, 126]. Like diamond, they are hard, insulator, optically transparent, and chemically inert, and are used in a wide range of applications, including low cost substitute for diamond [127-130].

There are variety of methods used to obtain DLC, such as CVD, pulsed laser deposition, sputtering, and ion beam deposition. The properties depend strongly on the growth conditions.

Like diamond, they have been extensively used as electrode material in biosensors [131-134]. However, there have not been efforts to utilize them for gas sensing as diamond films discussed above, and there exists a good scope to take advantage of their lower cost.

1.6.8 Chemical sensors based on conductive carbon films

An alternative to carbon nanotubes and nanowires is carbon nanofilms for developing miniature sensing devices. In this respect, amorphous conductive carbon nanofilms which lack order in their material structure can be useful for sensor application for their easy preparation [5, 57-59, 135-140]. This is especially true, if exact reproducibility of the sensor devices is not sought. Amorphous carbon film based ammonia sensors [139] and moisture sensitive sodium or potassium doped carbon films were previously reported [138, 140]. However, not much attention has been paid to carbon films as sensor material for other vapors or gases. More recently, graphene has been shown to perform well for sub-ppm level detection of different gases [60, 61]. However, practical application of graphene as sensing material faces the challenges of stability and compatibility with insulating substrates.

1.6.9 Graphite/Diamond-hybrid systems

Among numerous methods available to synthesize conductive amorphous carbon films, surface conversion of diamond at high temperatures is of special interest [5, 141-143]. The as-grown carbon films on diamond can further be treated by plasma to obtain desired chemical sensitivity. This approach is different from obtaining carbon sensing material on other non-carbon substrates and provides a unique natural combination of two carbon materials with complementary electronic properties: conductive amorphous carbon nanofilm and perfectly insulating diamond substrate.

In addition to acting as an insulator which may be employed in extreme conditions for its mechanical strength and chemical inertness, the thermally conductive diamond can also dissipate heat generated in such systems much efficiently. This makes diamond an ideal

substrate and graphite/diamond system an excellent choice for electronic applications.

This may also be considered as an all-carbon technology and hence important in light of an increased interest in carbon due to growing environmental concerns. Carbon is known to be a biocompatible material and is generally conceived suitable for biological and medical applications [144-151].

However, the related applications have not been explored probably because of the involved cost and technological complexities in making practical devices. The graphitic carbon on diamond may be considered as a natural basis for development of all-carbon sensors, which could be promising for biological and medical applications.

a. High temperature graphitization of diamond

The diamond is thermodynamically metastable at normal pressures and temperatures, and undergoes phase transformation to graphite at high temperatures. However, the kinetic of the process is much slow and needs temperatures higher than 1000 ^{o}C to show any detectable change and a non oxidative environment during the heating process.

In an earliest effort by Evan and James to determine the role of temperature in graphitization, diamond fragments were heated in the temperature range of 1500 - 1900 ^{o}C [141]. Transmission electron microscopy of the surface showed steep dependence of graphitization rate on temperature. Small crystallites of graphite observed after heating for 45 min at 1500 ^{o}C covered the surface completely when heated at 1900 ^{o}C for just about 5 – 10 min. Further, the size of graphitic crystallites varied between 100 and 150 A^{o} with orientations determined by the nature of the diamond surface. Nucleation and movement of dislocations from the diamond-graphite interface was suggested as the part of the partial graphitization surface. In this regard, the dynamic study of graphitization by in situ measurement of conductance in an inert atmosphere, as reported in the dissertation, is first

such study.

Another important study suggested the graphitization starting at the surface, with the formation of the precursor sites by surface reconstruction. This reconstruction is the rate determining step and conversion to graphite that follows is much faster. The conclusion was based on the rapid graphitization of an otherwise resistive diamond surface at a specific temperature, on bombardment with argon ions. It was believed that the disrupted sites modeled the precursor sites of high temperature graphitization process. It may be noted that ion bombardment is another way to graphitize diamond, discussed later in the chapter. In the present case energy of the ions were kept low enough to avoid direct graphitization.

Size dependent metastabilty of diamond is also known; diamond when smaller than one micron may easily transform to graphite at normal temperatures [152]. The enormously high pressure is needed to maintain stability at such lower sizes. Under high pressure high temperature (HPHT) conditions employed for growth of diamonds, diamond seeds preferentially converted to graphite when of few nanometer size. Such metastable states are not suitable for surface graphitization, and the complete graphitization of the material takes place.

Theoretical studies of graphitization of diamond by molecular dynamics method have also been performed. The method, limited by availability of computational resources, has successfully been able to simulate conversion of nanodiamonds containing about 2000 atoms to onion like carbons. The calculated amount of residual sp^3 carbons was about 17 % and accounted for the corresponding signal in different experimental characterization.

b. Graphitization by ion bombardment

The bombardment of diamond surface with high energy ions is a well known method to create lattice defects, and used to tailor its electronic and optical properties [153-157]. At sufficiently high energies, the severe bonding disruptions lead to graphitization near the impact area [158-170]. Zaitsev et al developed a technique based on this principle which utilized focused ion beam (FIB) to write nanostructures of graphitic carbons on diamond with nanometer precision [171-173]. The technique was used to construct chemical and temperature sensors based on arrays of carbon nanowires on diamond [172, 173]. However, the high cost of FIB technology hinders its use for scalable production of practical devices. Also, for obtaining graphitic nanofilms on diamond, high temperature heating, which involves conversion of whole surface, is more suitable.

Chapter II

Experimental design and Methodology

2. 1 Growth of carbon nanofilms on diamond

Carbon nanofilms were grown on diamond samples using high temperature annealing in vacuum or inert atmosphere. Polished, optical grade single crystal and polycrystalline diamond plates of size 2.5×2.5×0.5 mm^3 grown by chemical vapor deposition were used for this purpose (supplied by Element6). Initial surface roughness of the samples was below 30 nm (specification of Element6). The crystallographic orientation of the surfaces of the single crystal samples was (100). Before annealing, the diamond samples were ultrasonically cleaned in acetone. Annealing was performed in steps at different temperatures in the range 700 – 1400 °C for 10–30 minutes at each step. At temperatures above 1000 °C, a conductive gray film of carbon started to form on the sample surface. A scheme of the process is presented in Fig. 2.1.

A home-made vacuum furnace was used for annealing in vacuum. Sample container and heater of the furnace were made of high purity graphite. The diamond plates were annealed at two different levels of vacuum: about 3×10^{-5} mbar and 3×10^{-2} mbar, which we further refer as high vacuum (HV) and low vacuum (LV).

For the annealing in gaseous atmospheres, a Sentronic furnace with horizontal alumina tube was used. Inert atmospheres were attained by purging the tube with ultrapure argon or nitrogen at a flow rate of about 1 L/min.

Recovery of diamond surface: The insulating surface of the diamond film was recovered by removal of the conducting carbon film on the surface using one of these methods: chemical etching, plasma etching, or physical abrasion. In chemical etching,

diamond plate was dipped in a mixture of concentrated sulfuric acid and $K_2Cr_2O_7$; the film was removed by strong oxidizing action of the mixture. Alternatively, carbon film was also removed by the prolonged plasma exposure. Physical abrasion method involved using diamond abrasive to mechanically remove the film.

2.2 Deposition of carbon nanofilms on insulating substrates

The carbon films were deposited on single crystalline quartz plates (z-cut, 5×5×0.5 mm^3) by the sputtering of carbon. A Cressington carbon coater was used for the purpose. The quartz plates were cleaned by sonicating them in ethanol and acetone for about 10 minutes prior to deposition. The deposited carbon films were annealed at different temperatures for 1hr and a pressure of about 2×10^{-5} mbar was maintained throughout the course of heating. Annealing was done in a specially designed high temperature furnace with a graphitic core. The graphitic core of the furnace helped prevent possible contamination of the carbon films by formation of metal carbides at high temperatures.

2.3 Plasma etching

Plasma etching is a widely used technique for the modification of diamond surfaces [174-184]. As-grown carbon films on diamond were successively thinned by etching in low pressure, low power air or oxygen plasma excited in Diener Electronics Pico-RF plasma etcher. To study the effect of plasma exposure in different gases, plasma chamber was filled and emptied several times by the respective gases for maximum purity, and a pressure of about 3 mbar at a moderate plasma power was maintained during the exposure.

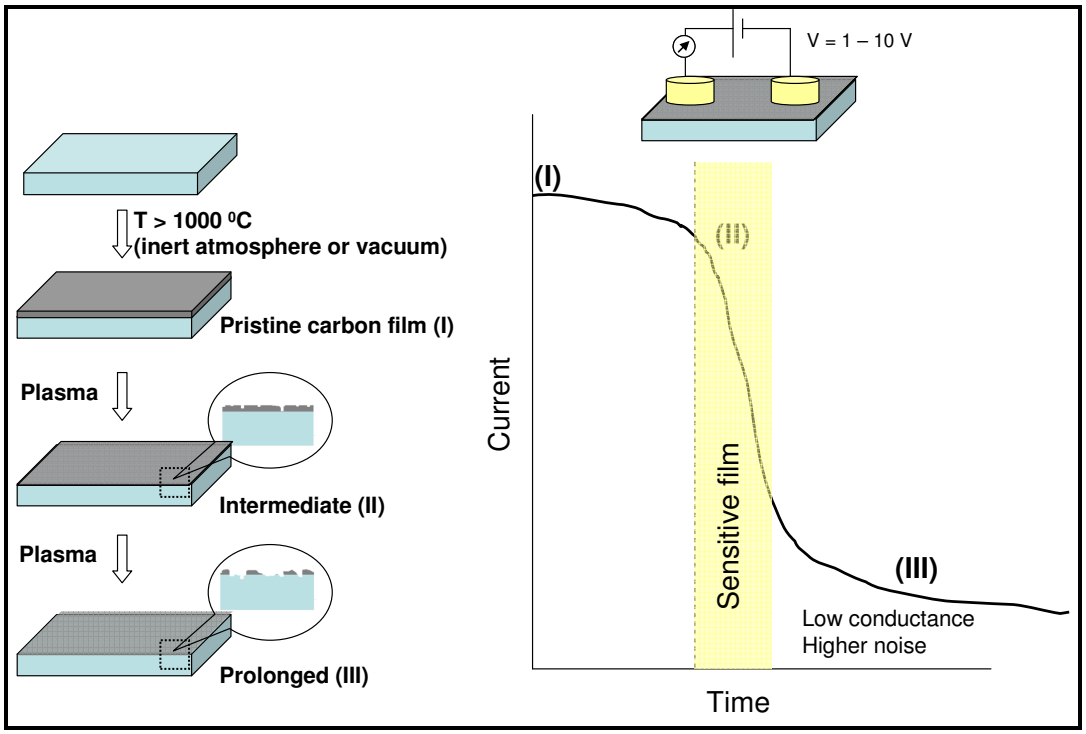

Fig. 2.1. Scheme of the growth of the carbon film on quartz and etching by plasma.

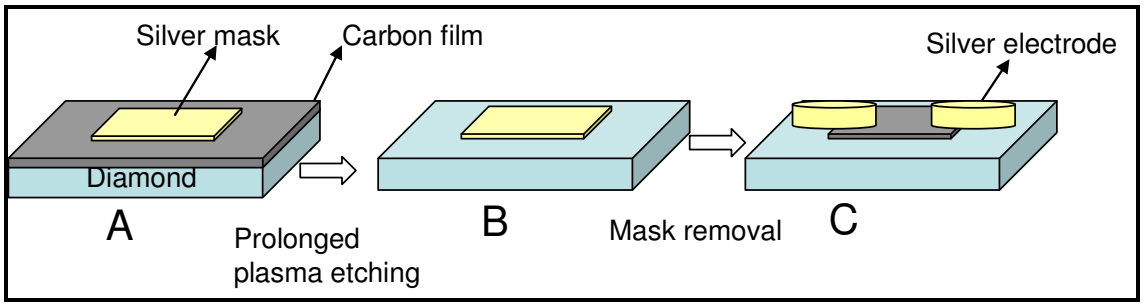

Fig. 2.2. Scheme of the preparation of the carbon film on diamond for AFM imaging and electrical characterizations.

2.4 Electrical characterization

Electrical conductance of the carbon nanofilms was measured at different stages of their growth and plasma treatment. For this purpose, a Keithley 4200-SCS semiconductor characterization system was used. The electrical characterization of the carbon films was done using a Keithley 4200 semiconductor characterization system. The conductance was measured using a specially designed ceramic holder with graphite electrodes, under the flow of dry nitrogen gas. The two graphite rods were directly placed over the bare film surface in a cylindrical alumina tube of a SentroTech tube-furnace. For some experiments conductance measurements were performed in open air using tungsten tips on the silver contact pads made on the carbon film.

The temperature dependence of conductance of carbon films and in situ graphitization of diamond, both were studied using specially designed ceramic holder under the flow of dry nitrogen gas. The samples were heated at about 8 ^{o}C / min and conductance was recorded with the changing temperature. The maximum heating temperature for temperature dependence study was set lower than the lowest annealing temperature (400 ^{o}C), to avoid any further permanent structural changes. While, for in situ graphitization, the maximum temperature was set around 1250 ^{o}C. The cooling rate was also maintained at about 8 ^{o}C / min.

2.5 Raman spectroscopy

For carbon films on diamond, Raman spectra were measured at room temperature using a confocal micro-Raman spectrometer Jobin-Yvon T 64000. Argon laser working at wavelength 488 nm was used for the excitation. The power of the laser beam at the sample surface did not exceed 5 mW. Raman spectra of the carbon films were obtained using

BrukerOptics MultiRAM Raman spectrometer at an excitation wavelength of 1064 nm. The laser power at the sample was set at 200 mW and data was collected at a spectral resolution of 2 cm^{-1}. Raman spectra of the carbon films on quartz were obtained using BrukerOptics MultiRAM Raman spectrometer at an excitation wavelength of 1064 nm. The laser power at the sample was set at 200 mW and data was collected at a spectral resolution of 2 cm^{-1}.

2.6 Atomic force microscopy

In order to estimate the conductivity/resistivity of the films their thickness was measured by an atomic force microscope (Asylum MFP 3D-Bio AFM) instrument working in tapping mode. A portion of the film was masked by silver paint and remaining portion was removed by plasma etching. After removal of silver paint mask, the step formed between bare diamond surface and carbon film was measured by AFM. The respective scheme is illustrated in Fig. 2.2.

2.7 Chemical sensitivity measurement

The chemical sensitivity of the carbon films was studied using a homemade apparatus (Fig. 2.3). The measurement was based on the change in conductance of the films on interaction with the vapors of analyte. Two silver contact pads were made on a carbon film and the sample was placed on the Teflon platform inside the testing-chamber. Pure dry nitrogen gas or argon (F2) was bubbled through the liquid analyte and the analyte vapor was diluted with another flow of the pure gas (F1). The diluted vapor was flown through the chamber alternatively at 100 s intervals by the alternate opening and closing of valve V3. A total flow rate of about 800 mL /min (F1 + F2) was maintained throughout. A voltage bias of

1 V was applied across the contact pads, and the conductance of the film as it changed during the exposure cycles was recorded.

Sensitivity to NO_2 and NH_3: Pure dry nitrogen gas was bubbled through concentrated solution of nitric acid / ammonium hydroxide and the gas carrying the respective vapors was diluted with another flow of dry nitrogen gas (F1). NO_2 resulted from the decomposition of HNO_3 ($4\ HNO_3 \rightarrow 4\ NO_2 + O_2 + 2\ H_2O$) and aqueous ammonium hydroxide solution released NH_3. It may be noted that sensitivity to water vapor (present in the analyte vapor) was negligible in comparison to NH_3 and NO_2, when measured separately with same flow of nitrogen gas. Sensitivity measurements were performed at a certain fixed concentration of the analyte vapors (different for NH_3 and NO_2) by maintaining a constant bubbling flow rate (F2).

Sensitivity to organic solvents or water: The vapors of organic solvents or water were produced by bubbling dry nitrogen/argon gas through the respective liquids. The vapors were further diluted by mixing with another flow of dry nitrogen/argon gas at different flow rates in order to vary the vapor concentration. The concentration ranges were thus limited by the vapor pressure of respective solvents at room temperature.

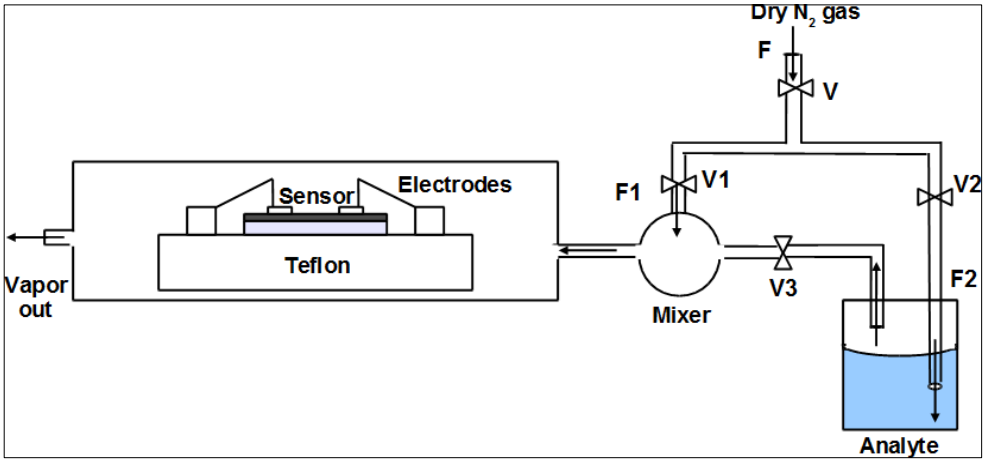

Fig. 2.3. Schematic of the chemical sensing test apparatus.

2.8 Temperature sensitivity measurement

For temperature dependence of conductance, the films were heated at about 8 ^{o}C / min and conductance was recorded with the changing temperature. The maximum heating temperature was set lower than the lowest annealing temperature (400 ^{o}C), to avoid any further permanent structural changes. The measurement of temperature sensitivity of carbon films on diamond was also carried out in open air by heating in the steps of about 2 ^{o}C, and letting the temperature stabilize before measuring the conductance at each step.

Chapter III

Carbon nanofilms on Diamond

3.1 Introduction

Among numerous methods available to synthesize conductive amorphous carbon films, surface conversion of diamond at high temperatures is of special interest [5, 141-143]. The as-grown carbon films on diamond can further be treated by plasma to achieve desired chemical sensitivity. This approach is fundamentally different from obtaining carbon sensing material on other non-carbon substrates and provides a unique natural combination of two carbon materials with complementary electronic properties: conductive amorphous carbon nanofilm and perfectly insulating diamond substrate.

The chapter presents the important results on carbon films on diamond for all-carbon sensor application and involves in situ study of graphitization of diamond, plasma modification of carbon films in different precursor gases and its effect on temperature and chemical sensing, and was also published earlier [5]. The films are characterized by atomic force microscopy and Raman spectroscopy.

3.2 Growth temperature

Fig. 3.1 shows surface conductance of a diamond sample on successive steps of high vacuum annealing at different temperatures. Some samples showed a considerable increase in conductance after annealing at temperatures below 800 °C and a decrease after annealing at higher temperatures. The origin of this increase is still not clear. However, since it is sample

dependent, it cannot be ascribed to surface graphitization. A sharp irreversible rise in conductance at around 1000 °C observed on all samples indicates the onset of conversion. The conductance rapidly increases with further temperature increase. A visibly light gray film of fairly high conductance is obtained after annealing at 1300 °C.

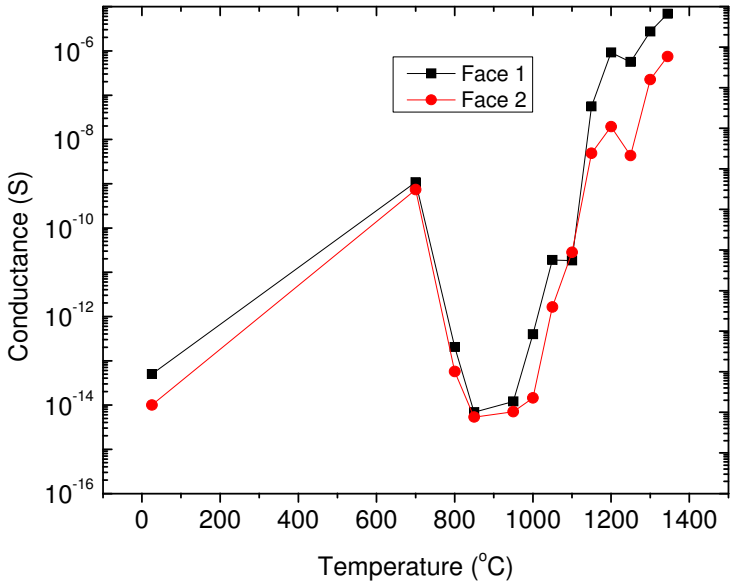

Fig. 3.1. Room temperature surface conductance of two faces of a diamond single crystal plate on successive annealing steps at different temperatures in high vacuum. The sample was annealed for 15 minutes at each temperature.

In order to find the temperature of the onset of the surface conversion in inert gas, in-situ measurements of the surface conductance were performed in the Sentronic furnace filled with nitrogen. Fig. 3.2 shows the change in conductance of single crystal diamond samples during heating and subsequent cooling. It can be clearly seen that the conductance induced by heating at a temperature of 1000 °C and above is stable and retains after cooling. All curves exhibit also a broad conductivity maximum at temperatures 600–700°C, which, we believe, is of the same origin as that shown in Fig. 3.1.

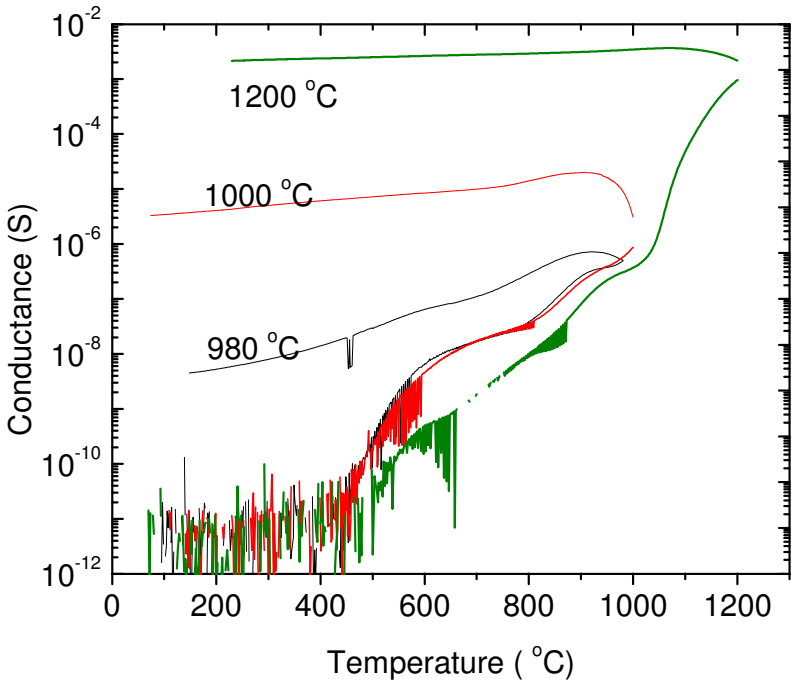

Fig. 3.2. In-situ measurement of surface conductance of diamond samples during the processes of heating and cooling in N_2 atmosphere with different maximum temperatures (indicated on the graph). For each process, the samples were kept at the maximum temperature for 15 minutes. Rate of cooling/heating was maintained at 5°C/min.

3.3 Electrical conductance of the films

The conductance of thin films grown in high vacuum at temperature 1200 °C for 15 min varied in the range 10^{-5}–10^{-4} S. Thick films obtained in low vacuum showed conductance in the range 10^{-4}–10^{-3} S. The conductance of the carbon films was also found to be influenced by the quality/type of the diamond samples. Thin films obtained on polycrystalline diamonds showed lower conductance at about 10^{-6} S.

The thickness of the films grown at temperature 1200 ºC for 30 minutes in high vacuum was found to be about 10 nm (Fig. 3.3), while that obtained at the same conditions but in low vacuum was about 100 nm (Fig. 3.4). Taking into account these thicknesses, specific resistivity of the films was calculated to be in the range 10^{-3}–10^{-4} Ω.m. This value, much higher than that of graphite (8×10^{-6}–15×10^{-6} Ωm) indicates the amorphous/discontinuous nature of the films.

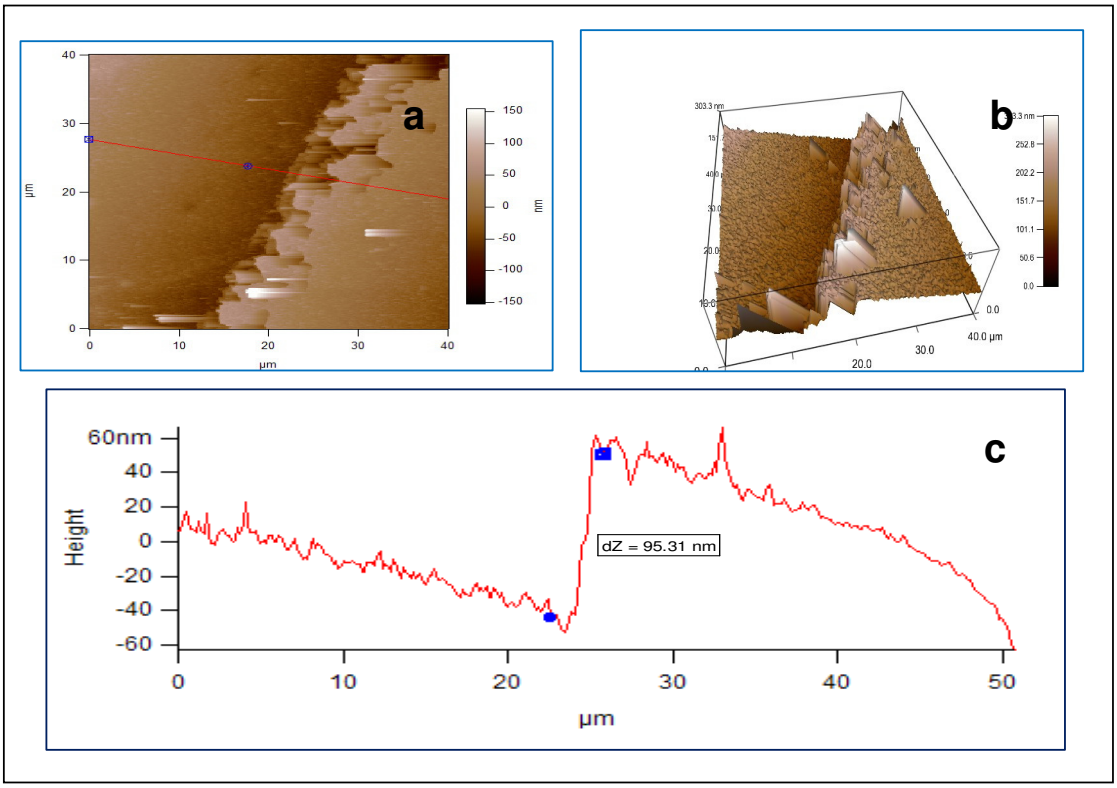

Fig. 3.3. AFM image (tapping mode) of edge of the carbon films grown on diamond surface by heating at 1200°C for 15 min in low vacuum (a, b), and surface profiles (c).

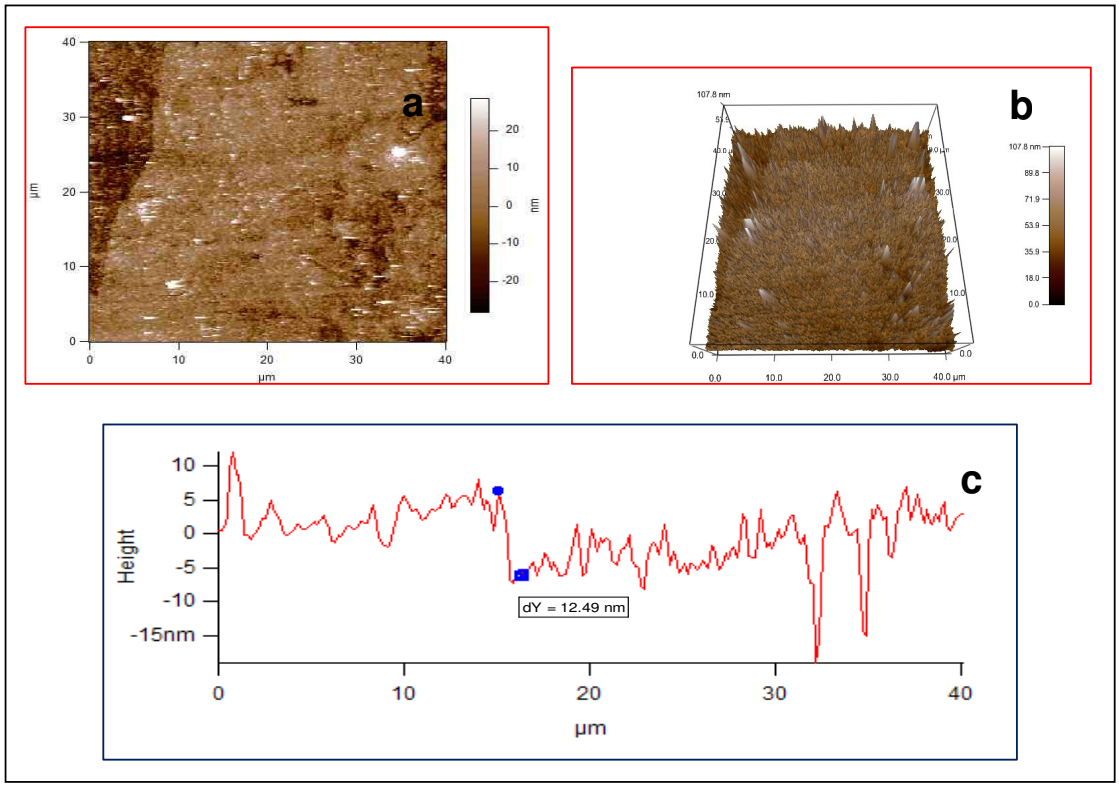

Fig. 3.4. AFM image (tapping mode) of edge of the carbon films grown on diamond surface by heating at 1200 °C for 15 min in high vacuum (a, b), and surface profiles (c).

The change in conductance of the carbon nanofilms exposed to plasma etching is shown in Fig.3.5. Plasma etching reduces conductance implying partial removal of conductive carbon. The change in conductance of thick films, grown in low vacuum, exhibits two distinctive regions. At the initial stages of etching (Region I), the conductance drops linearly with etching time, and then it reduces exponentially (Region II). A residual conductance is observed in the end on prolonged exposure (Region (III). Thin films, grown in high vacuum, show the exponential drop of conductance from the very beginning of the etching (Fig. 3.6).

A comparative study of the effect of hydrogen, oxygen, argon, and SF_6 on the surface conductance of the carbon film on quartz indicated a greater etching ability of hydrogen plasma followed by oxygen, and argon, in the order (Fig. 3.7). Interestingly, SF_6 was ineffective with no apparent decrease in conductance even after several hours (Fig. 3.8). Further, the current-voltage characteristics remained linear even after prolonged plasma exposures in different precursor gases, indicating unchanged ohmic character. Fig. 3.9 shows current voltage characteristics of plasma treated films having different levels of conductance, obtained by successive plasma treatments of the pristine carbon film: P1 ($\sim 10^{-5}$ S), P2 ($\sim 10^{-6}$ S), P3 ($\sim 10^{-7}$ S), P4 ($\sim 10^{-8}$ S). P0 is the initial pristine carbon film.

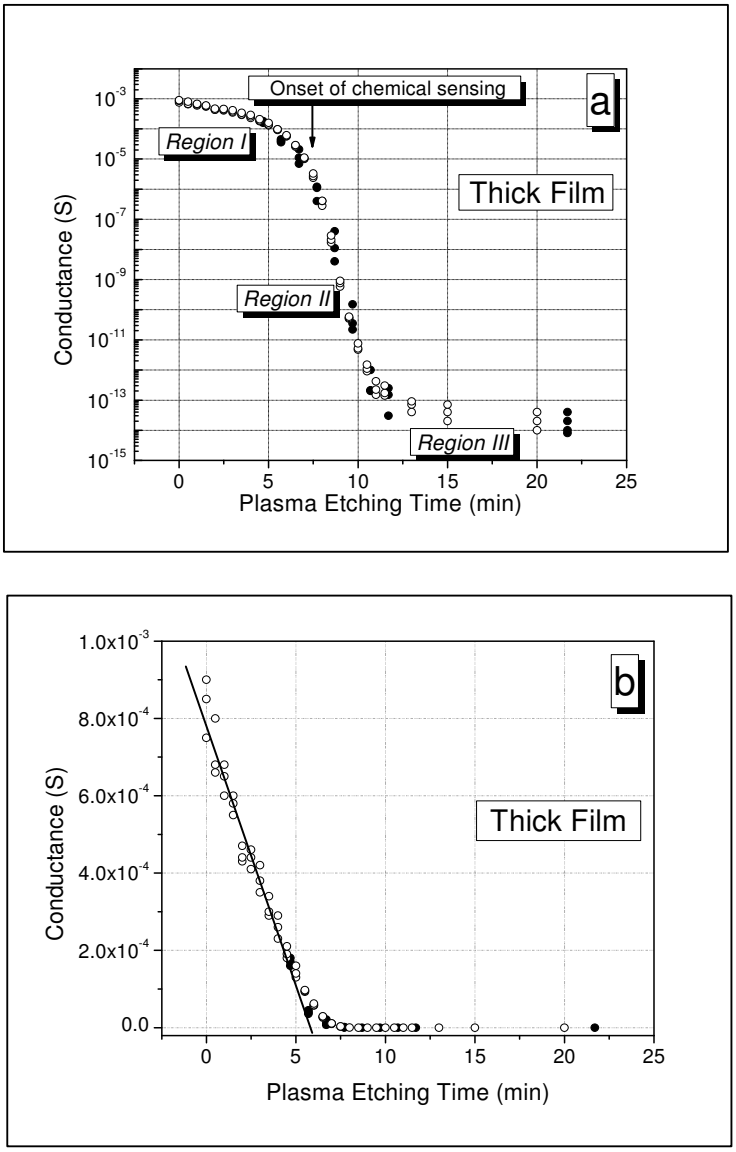

Fig. 3.5. Change in conductance of a thick carbon film on diamond surface versus time of treatment in air plasma. Thick film exhibits linear decrease in conduction at the initial stages of etching and exponential afterward. Reduction of conductance of thick film is shown both in logarithmic (a) and linear (b) scales to highlight the ranges of exponential and linear drops.

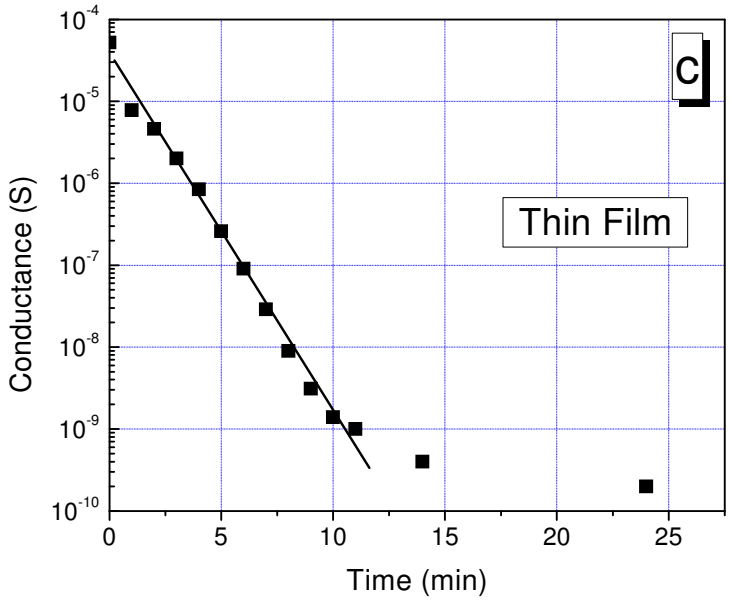

Fig. 3.6. Change in conductance of a thin carbon film on diamond surface versus time of treatment in air plasma. Thin film shows exponential decrease of conductance from the very beginning of etching.

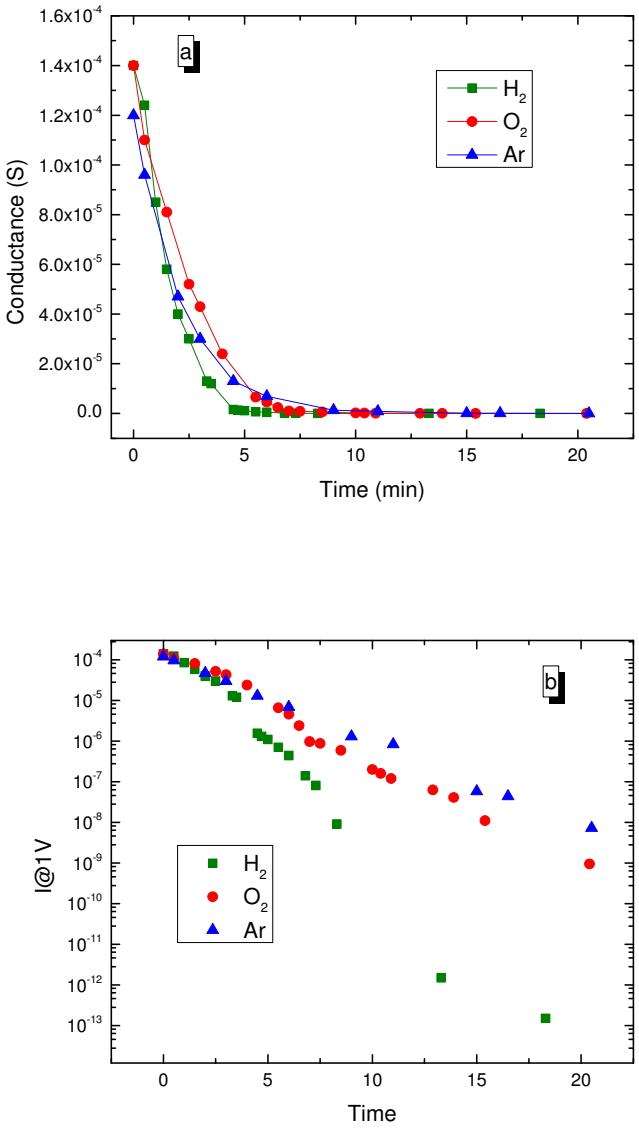

Fig. 3.7. Change in conductance of a thin carbon film on diamond on treatment in different plasma atmospheres, shown both in logarithmic (a) and linear (b) scales.

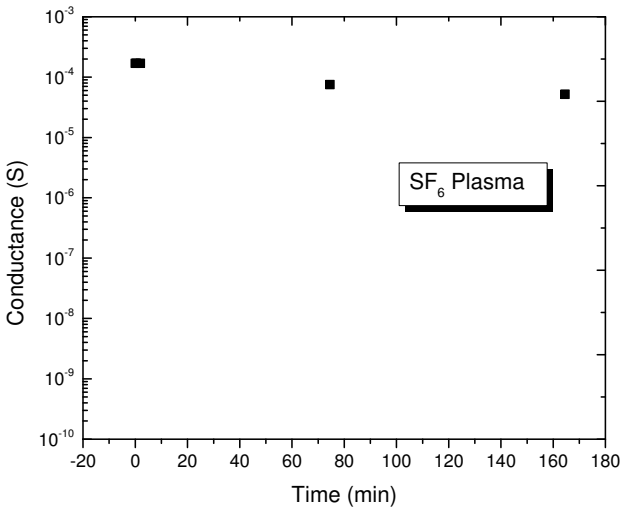

Fig. 3.8. Change in conductance of a thin carbon film on diamond on treatment in SF_6 plasma, shown both in logarithmic (a) and linear (b) scales.

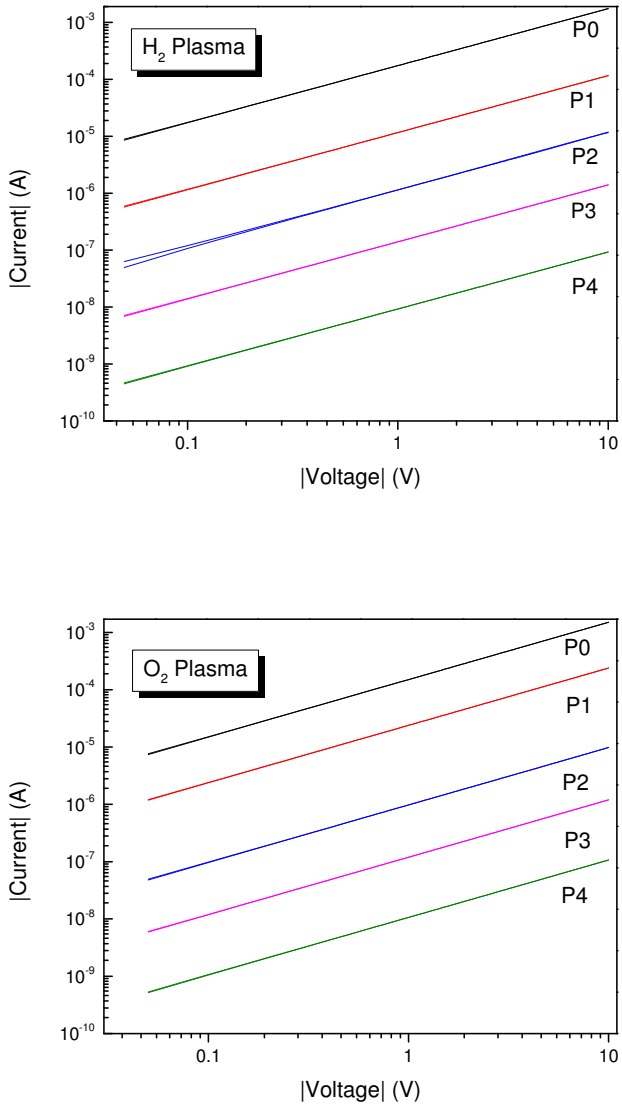

Fig. 3.9. Current voltage characteristics of plasma treated carbon films on diamond having different levels of conductance, obtained by successive plasma treatments of the pristine carbon film: P1 (~10^{-5} S), P2 (~10^{-6} S), P3 (~10^{-7} S), P4 (~10^{-8} S). P0 is the initial pristine carbon film.

The decrease in conductance with time of plasma etching is attributed to successive removal of the conductive layer from diamond surface. We believe that after the film was removed there might have been some conductive carbon still trapped between the surface features as indicated by a residual surface conductance, resulting into formation of a random array of isolated carbon nanodots (Fig. 3.10).

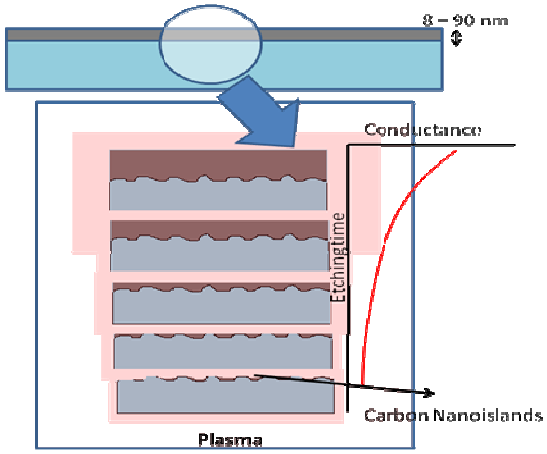

Fig. 3.10. Cartoon depicting the transformation of carbon film on diamond surface during exposure to plasma. A discontinuous random array of carbon nanoislands on diamond surface is assumed to be formed after prolonged exposure.

3.4 Raman characterization

In order to gain more insight into nature of the carbon nanofilms grown on diamond surface, Raman spectra were measured on as-graphitized diamond surface and after successive plasma etching (Fig. 3.11). The characteristic D and G bands at wavenumbers 1350 and 1590 cm^{-1} indicate the presence of amorphous carbon [185, 186]. As the films are etched by plasma and their thickness decreases, both bands become broader and shift one

towards another eventually merging into one weak broad band at a wavenumbers of 1450 nm. We speculate that with plasma etching, the carbon nanofilms become increasingly amorphous.

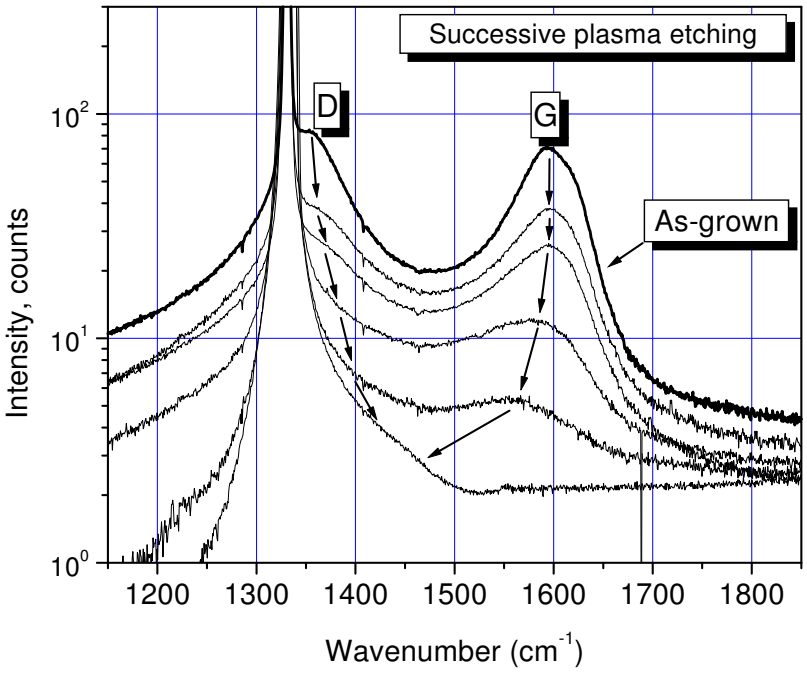

Fig. 3.11. Raman spectra of thin carbon nanofilm as-grown and after several steps of successive plasma etching. Each etching step was about 1 minute.

3.5 Temperature sensitivity

Conductance of the carbon nanofilms of varying thicknesses, obtained by plasma etching, was studied for its temperature sensitivity Fig. 3.12. The conductance of all films increased with heating with no permanent change in conductance. The magnitude of the temperature-induced increase in conductance depended considerably on the film thickness. The conductance of as-grown thick films remained high and almost temperature independent, while that of the as-grown thin film was lower and showed slight increase with temperature. Depending on the plasma power, it may take up to 30 minutes of plasma exposure to reduce the conductance of the thick film by three orders of magnitude and thus to make it comparable with that of the as-grown thin films. The plasma etched thick film was found to be nearly as sensitive to temperature as the as-grown thin film. The etched thin film (1.5 min of plasma exposure) showed nearly 3 times increase in conductance on heating from room temperature (0.18 μS) to 150 ºC (0.43 μS). Further etching for another 1.5 min causes further reduction in the overall conductance level and increase in the temperature sensitivity. On continued etching, the conductance was lowered down to 10^{-10} S and its temperature change raised to one order of magnitude.

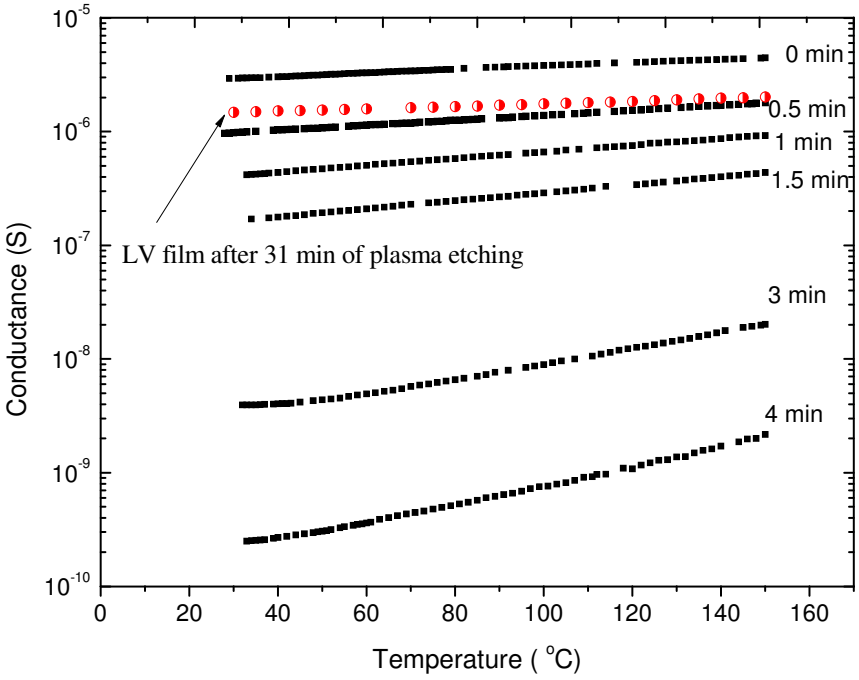

Fig. 3.12. Temperature dependence of conductance of a thin carbon nanofilm: as-gown (upper curve) and after plasma etching for times indicated in the graph. Change in conductance of a thick carbon film after 31 min of plasma etching is also included for comparison (red curve).

The temperature sensitivity was examined in terms of the models of the temperature activation via energy barrier E_a, and variable range hopping [187-189]. The temperature activation via energy barrier is approximated by simple dependence:

$$G(T) = G_o \exp(-E_a/kT), \qquad (1)$$

where, T is the absolute temperature, k is the Boltzmann constant, E_a is the activation energy and G_o is a constant. The conductance shows increasingly exponential dependence as film is etched by plasma. However, for very thin films, the observed trend significantly deviates from the exponential dependence over the temperature range (Fig. 3.13a). Empirically, this

deviation may be described by the change in activation energy with temperature. Fig. 3.13b shows that for plasma etched films the activation energy changes almost exponentially on heating, while it remains almost constant for as-grown films.

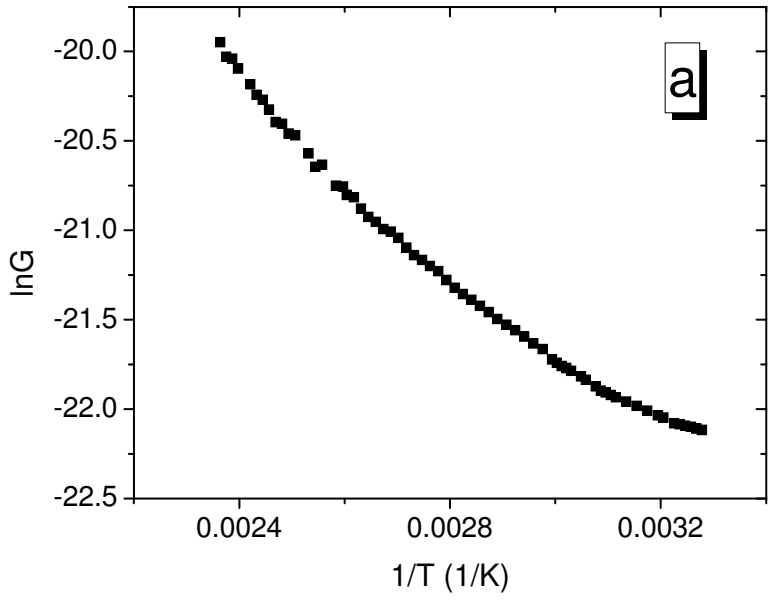

Fig. 3.13. (a) Logarithm of conductance of a plasma etched thin carbon nanofilm (4 min of plasma etching at a moderate power level) as a function of T^{-1}. (b) Temperature dependence of activation energy for as-grown thin film and plasma etched films. The dependence is increasingly exponential on plasma etching (increased slope of best-fit line on logarithmic scale).

The simulation of the temperature sensitivity based on the variable-range-hopping model is performed using the relation:

$$G(T) = G_o \exp(-T_o/T)^{1/4}, \qquad (2)$$

where T_o is the hopping temperature and G_o is the conductance prefactor. However, when we

plot conductance G on logarithmic scale vs. $T^{-1/4}$, there is only minor improvement in the fit over the simple form given by Eq. (2), at least for the very thin films (Fig. 3.14a). Thus, we may conclude that none of the two mechanisms mentioned above is the major one driving the temperature stimulation of conductance of plasma-etched carbon nanofilms on diamond. Instead, we found that the temperature change in conductance shows the best fit when simulated by dependence:

$$G(T) = A \exp(BT), \qquad (3)$$

where, B is an empirical constant (slope of the best fit line), which increases on plasma thinning, for both as-grown and plasma etched films (Fig. 3.14b). Same dependence was observed on carbon nanostructures made on diamond surface by irradiation with focused ion beam [172, 173]. More studies are needed to understand this particular behavior.

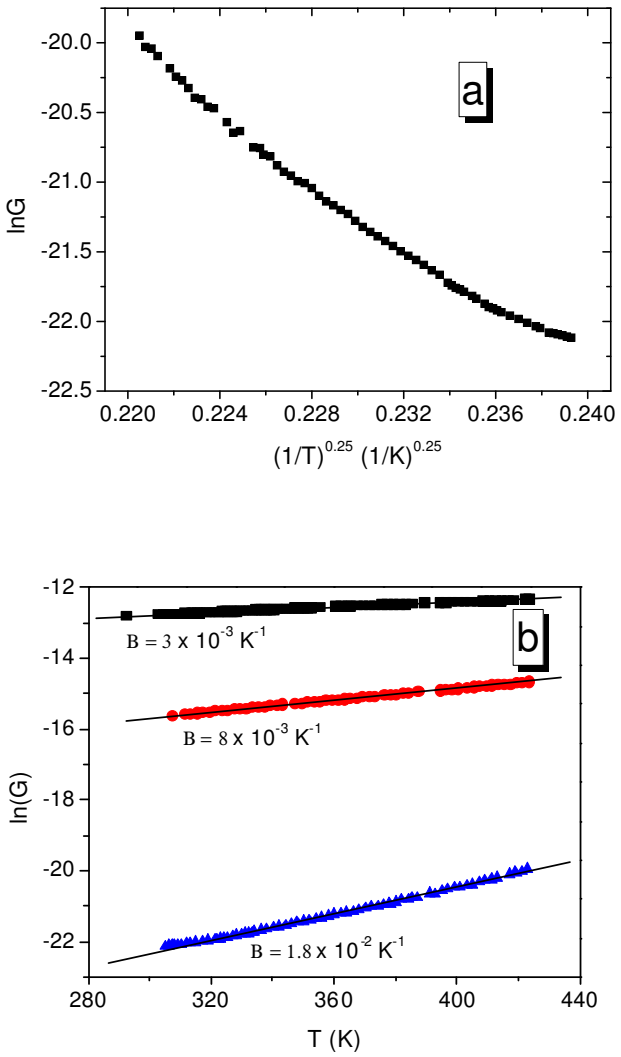

Fig. 3.14. (a) - Logarithm of conductance of a thin plasma etched film as a function of $T^{-1/4}$. (b) Comparison of temperature dependences of conductance of as-grown, intermediate and thin plasma etched films as a function of T. The intermediate and thin plasma etched films were obtained by 1.5 min and 4 min plasma etching respectively.

3.6 Chemical sensitivity

Thin carbon nanofilms, and especially those obtained after plasma etching, revealed appreciable chemical sensitivity for different gaseous analytes. Fig. 3.15 and Fig. 3.16 show the response transients and sensitivity (the relative change in conductance; $\Delta G/G_o$) of plasma etched films on exposure to varying concentrations of water and acetone vapors, respectively. G_o is the conductance in pure dry argon gas. The films with different levels of conductance are compared. Response to water steadily increases with increase in the water vapor concentration (Fig. 3.15). The sensitivity of as-grown film to water vapor is only 0.1 at the maximum vapor concentration (1.5%). However, after plasma etching, the sensitivity of the film to the same vapor concentration increases to 1.5.

Response to acetone vapor is different as compared to water (Fig. 3.16). Firstly, it is much less than that to water. Acetone could produce same sensitivity of 1.5 only at a vapor concentration of 14%. Secondly, thick films revealed almost constant sensitivity of 0.02 independent of the acetone vapor concentration. Thirdly, sensitivity of thin plasma etched films was not monotonous and exhibited a maximum at a certain vapor concentration (Fig. 3.16b).

The recovery time of the film conductance after the supply of the analyte vapor into the chamber has been shut down was about 1 minute. Though the reported results are for acetone and water vapors, we have found similar response and recovery time for vapors of alcohol, NO_2 and NH_3. Such a sort recovery time is remarkable when compared to that of carbon nanotubes, which may be as long as 10 hours and an ultraviolet illumination is required to decrease it to a few minutes [32].

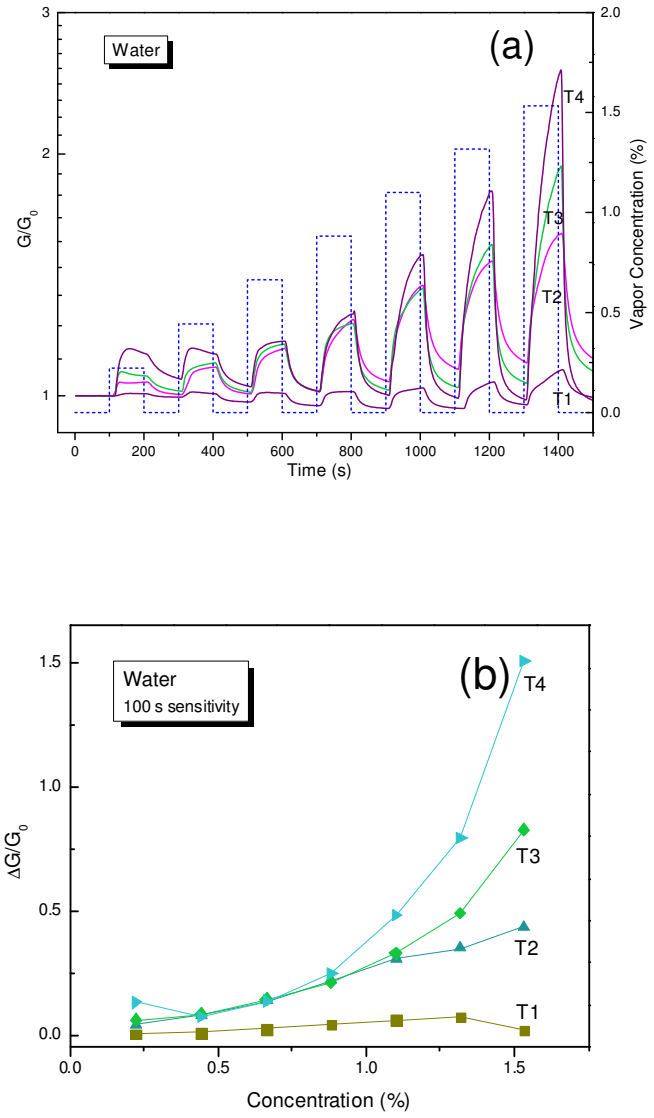

Fig. 3.15. Response of plasma etched carbon films on diamond, on exposure to varying concentrations of water vapors in dry argon gas. Curves T1, T2, T3 and T4 correspond to the films with conductance 2.1 x 10^{-7}S, 1.9 x 10^{-8} S, 1.9 x 10^{-9} S and 3.1 x 10^{-10} S, respectively; obtained by successive plasma etching. The dotted line shows the concentration cycles of analytes injected into measuring chamber with 100 s duration pulses.

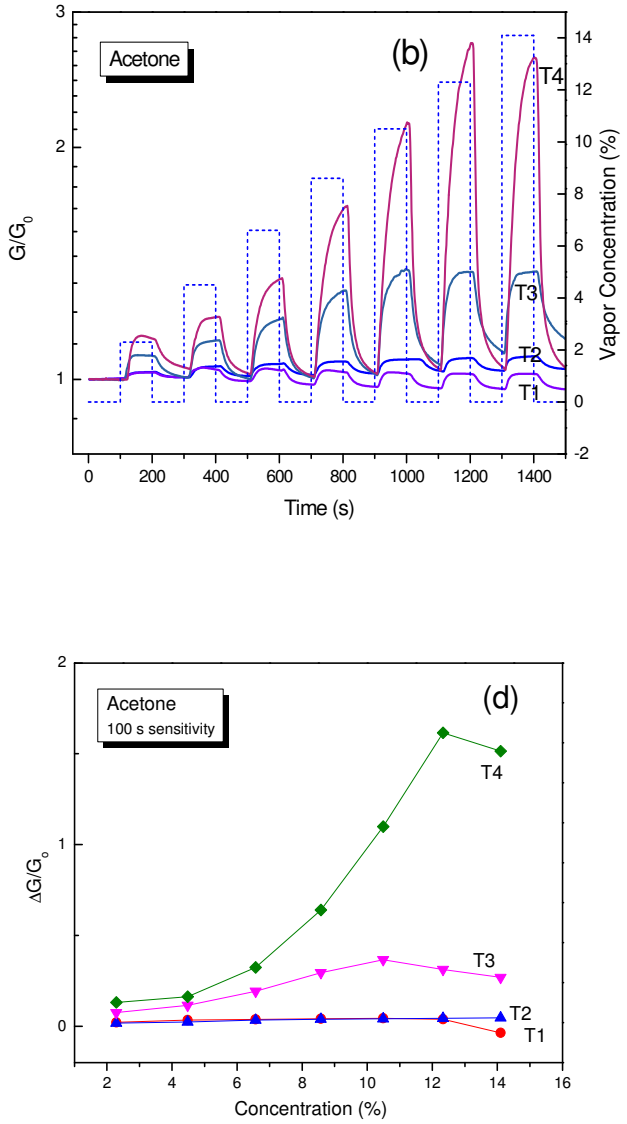

Fig. 3.16. Response of plasma etched carbon films on diamond, on exposure to varying concentrations of acetone vapors in dry argon gas. Curves T1, T2, T3 and T4 correspond to the films with conductance 2.1 x 10^{-7}S, 1.9 x 10^{-8} S, 1.9 x 10^{-9} S and 3.1 x 10^{-10} S, respectively; obtained by successive plasma etching. The dotted line shows the concentration cycles of analytes injected into measuring chamber with 100 s duration pulses.

Since the physical size of the carbon nanofilm chemical sensors can be very small (ultimately down to a few tens of nanometers), they can be used for the measurements of small objects. As an example, we measured response to water vapor surrounding a water droplet of a diameter of 1 mm using a carbon nanofilm sensor with an active area of a size of 100 microns. The water droplet was placed on the tip of a needle of micromanipulator and was moved precisely around the sensor. The sensor response, as a water droplet is approached and withdrawn is shown in Fig. 3.17.

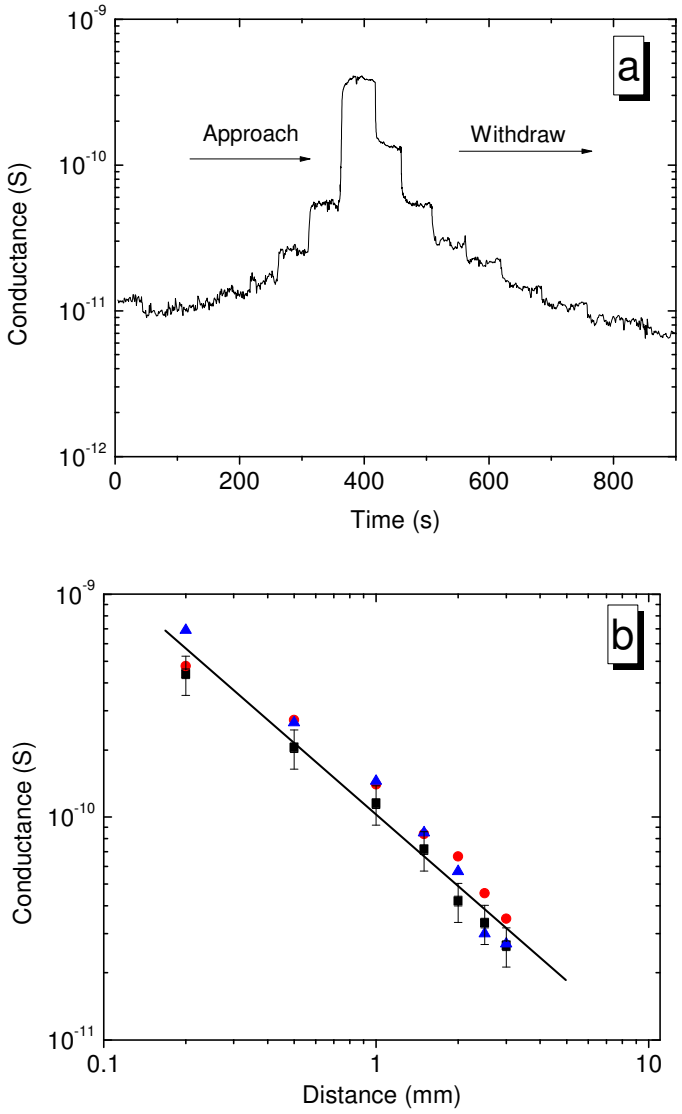

Fig. 3.17. (a) Change in conductance of a thin carbon nanofilm as a 1 mm diameter droplet of water is approaching and withdrawing the film in steps. The maximum distance is about 10 mm (the lowest conductance), and the minimum distance is a fraction of millimeter (maximum conductance). (b) The conductance of a thin carbon nanofilm versus distance between the water droplet and the carbon nanofilm sensor. The conductance increase is inversely proportional to the distance.

The conductance of the films remained ohmic at different levels of exposure to chemical analytes. Fig. 3.18 shows that the linear current-voltage characteristic of a carbon film does not alter as it is exposed to water vapor produced by a water droplet bought to the film surface at distances from 0.1 to 8 mm. This observation shows that the analyte vapor adsorbed of the carbon nanofilm surface does not form any energy barriers, which could result in current injection and non-linear current-voltage characteristics. Instead, the analyte molecules just increase/reduce concentration of charge carriers in the film. This behavior resembles the performance of a chemical field-effect transistor where the controlling gate voltage is created by the molecules adsorbed on the surface of conductive channel.

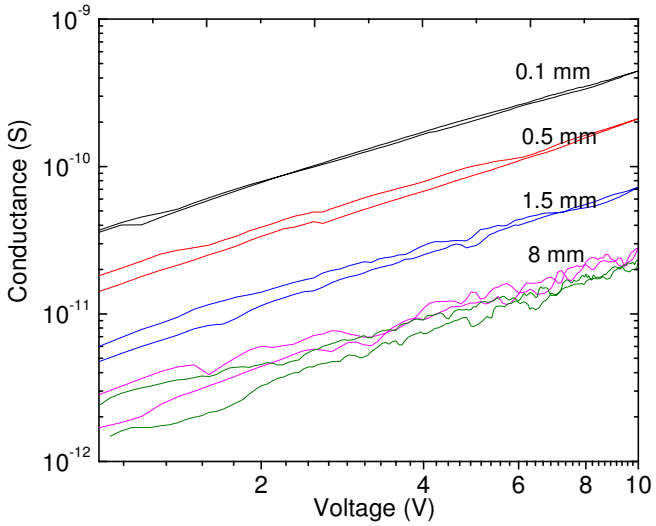

Fig. 3.18. Current-Voltage characteristics of a thin carbon nanofilm in the presence of a 1 mm diameter water droplet placed at distances specified.

3.6.1 Selective chemical sensing on plasma modification

The relative effect of hydrogen and oxygen plasma on chemical sensitivity was studied to determine their role in selective chemical sensing. The carbon films obtained by successive exposure in their respective plasmas, as in section 3.3, had different levels of conductance: P1 (~10^{-5} S), P2 (~10^{-6} S), P3 (~10^{-7} S) and P4 (~10^{-8} S). The films were exposed to varying concentrations of water, acetone, toluene, and hexane, and sensitivity was recorded at the different concentrations.

a. Pristine films

Sensitivities to toluene, acetone and hexane were negative, while for water, it was positive (Fig. 3.19). For a similar level of concentration (~2 %), sensitivity to toluene was maximum, more than 4 times acetone, which in turn was about 10 times hexane. The negative sensitivity increased almost 6 fold on increasing the acetone vapor concentration to 4 times. For toluene, increase was about 10 times for a similar increase in concentration. In comparison, sensitivity to water was positive and remained almost constant with concentration.

b. Hydrogen plasma

Fig. 3.20 and Fig. 3.22 summarize the effect of hydrogen plasma.

Water: Sensitivity to water increased slightly. For P1, P2, and P3, sensitivity remained almost constant, and sharp increase in sensitivity, almost 15 times increase at 2 % concentration, was observed when further etched. For, P4 almost exponential dependence on concentration was observed after a certain concentration (~1 %).

Acetone: Sensitivity remained negative and almost unaffected. However, for P4, the positive sensitivity increased with concentration in the beginning, and then decreased to a slight negative value after a certain maximum concentration (~9 %).

Toluene: A continuous increase in sensitivity at all concentration levels was observed. About 5 times increase from P1 to P4 for ~2 % concentration, and increasingly steeper rise in sensitivity with concentration was observed.

Hexane: The negative sensitivity changed to positive on plasma exposure, with no specific dependence on exposure time or concentration.

c. Oxygen plasma

Fig. 3.21 and Fig. 3.23 summarize results on the effect of hydrogen plasma.

Acetone: Almost constant to slight increase in sensitivity on initial plasma exposure, followed by a sharp increase when etched to P4 was observed. Further, for P4, the sensitivity was strongly dependent on concentration, and increased almost 40 times when concentration changed about 6 times.

Water: A steady increase in sensitivity and a sharp increase when etched to P4 were observed. Like acetone, sensitivity to water was strongly dependent on concentration for P4. At 1.5 % concentration, almost non-sensitive as-deposited carbon film showed sensitivity of 12 % at P3, which became as high as about 50 % for P4, about 14 times higher than P1.

Hexnae: Oxygen plasma treated films didn't show any specific trend in their sensitivity for hexane. However, P2 shows an interesting behavior with a maximum sensitivity of about 6% for the lowest concentration of hexane, which decreased exponentially with concentration indicating the role of surface passivation in sensitivity.

Toluene: No particular trend in sensitivity was observed, except the negative sensitivity became positive on plasma exposure.

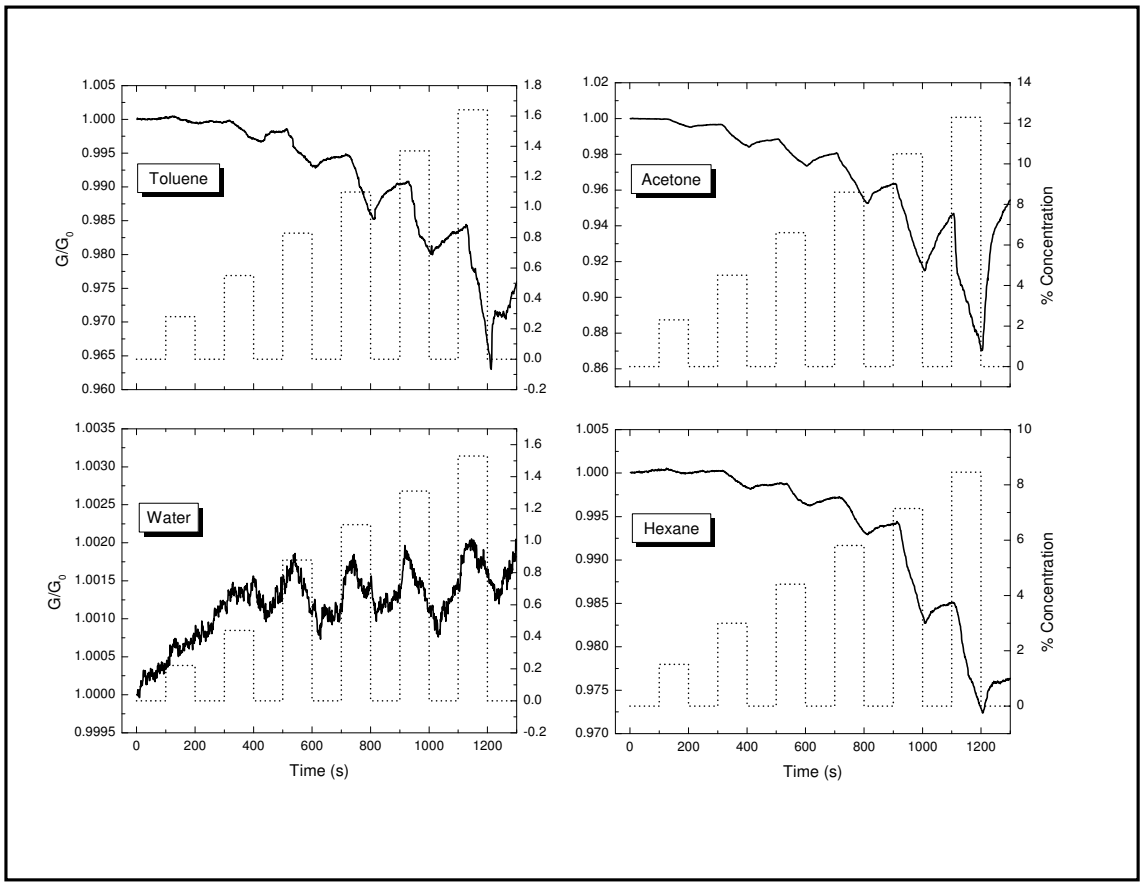

Fig. 3.19. Response of pristine carbon film on diamond to the varying concentrations of different vapors: toluene, acetone, water and hexane.

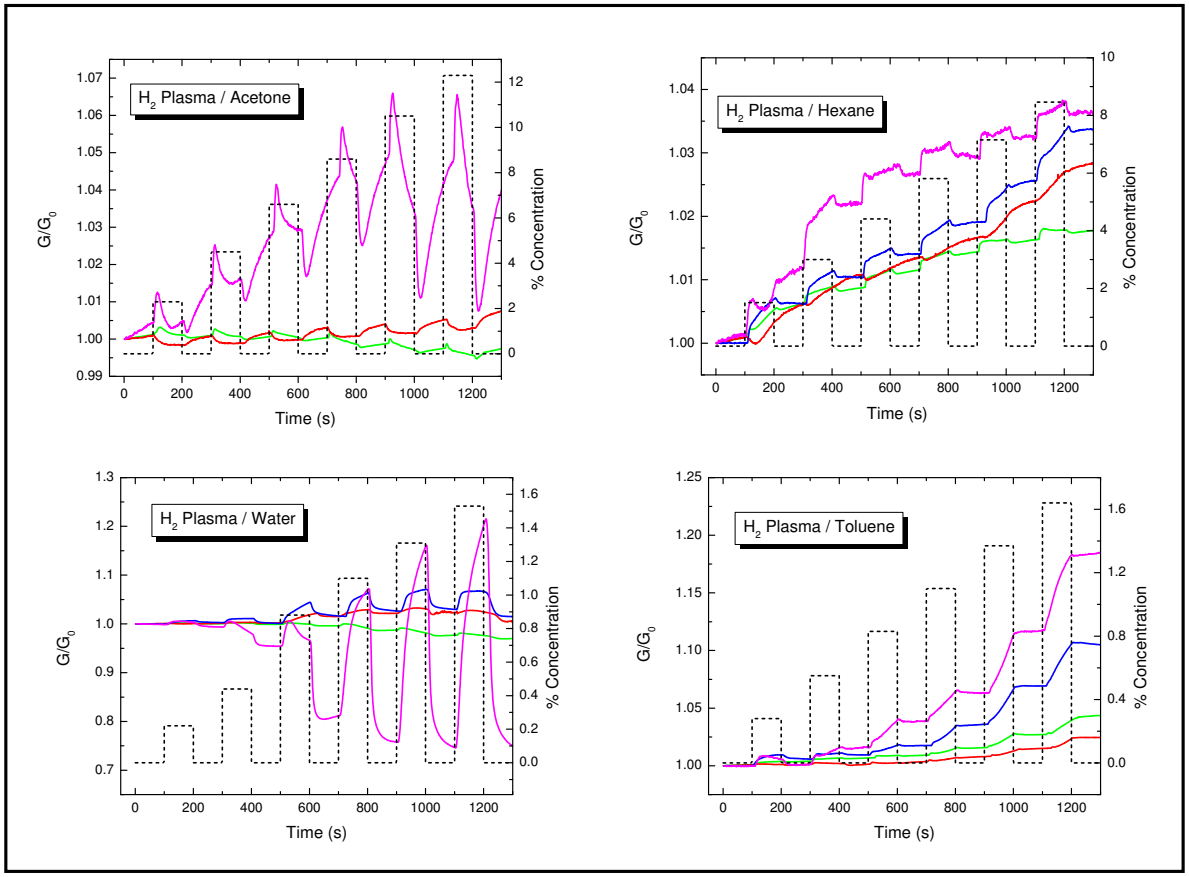

Fig. 3.20. Response of hydrogen plasma treated carbon films on diamond to the varying concentrations of different vapors: toluene, acetone, water and hexane. Green: P1 (~ 10^{-5} S), Red: P2 (~ 10^{-6} S), Blue: P3 (~ 10^{-7} S), Purple: P4 (~ 10^{-8} S).

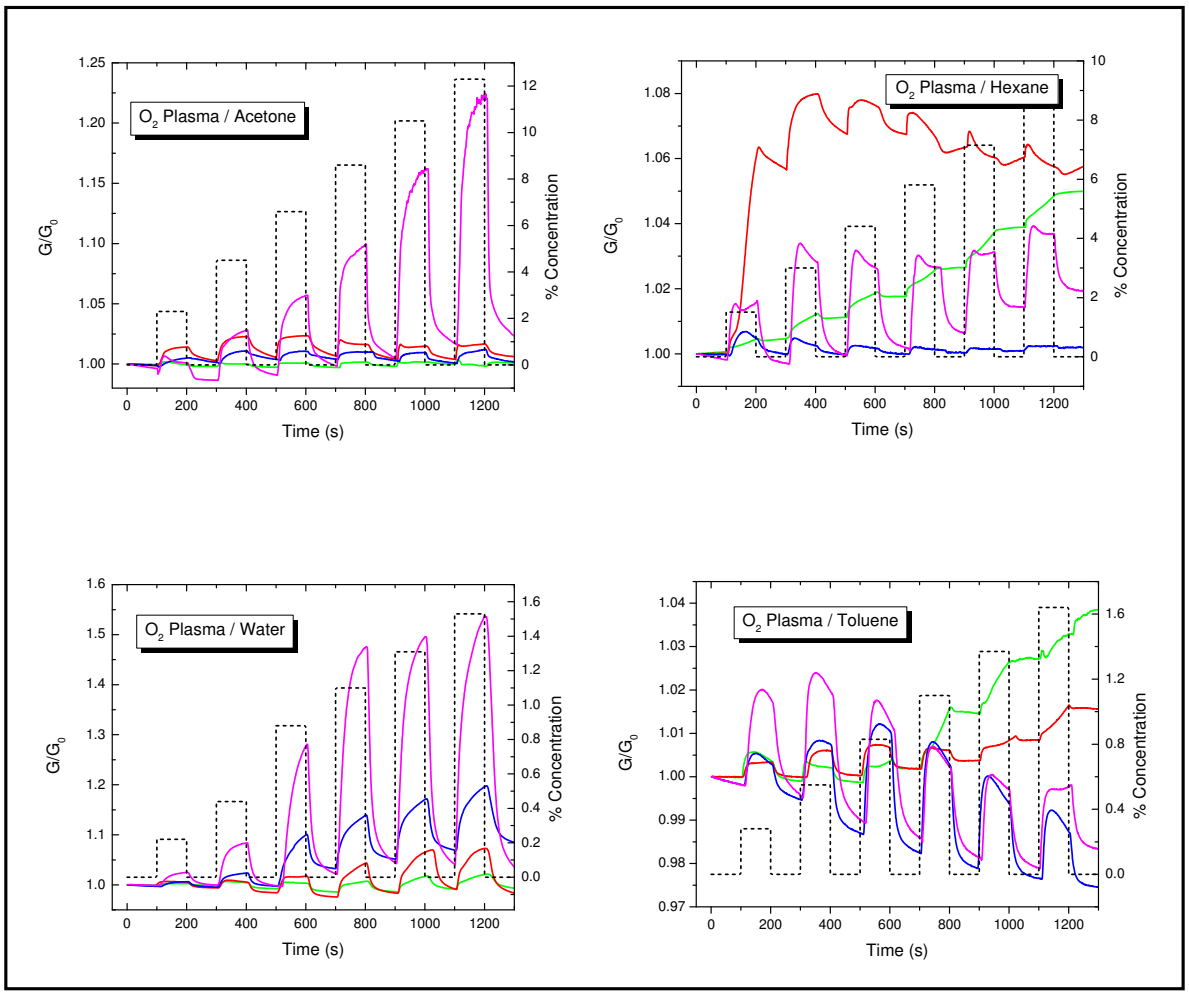

Fig. 3.21. Response of oxygen plasma treated carbon films on diamond to the varying concentrations of different vapors: toluene, acetone, water and hexane. Green: P1 (~10^{-5} S), Red: P2 (~10^{-6} S), Blue: P3 (~10^{-7} S), Purple: P4 (~10^{-8} S).

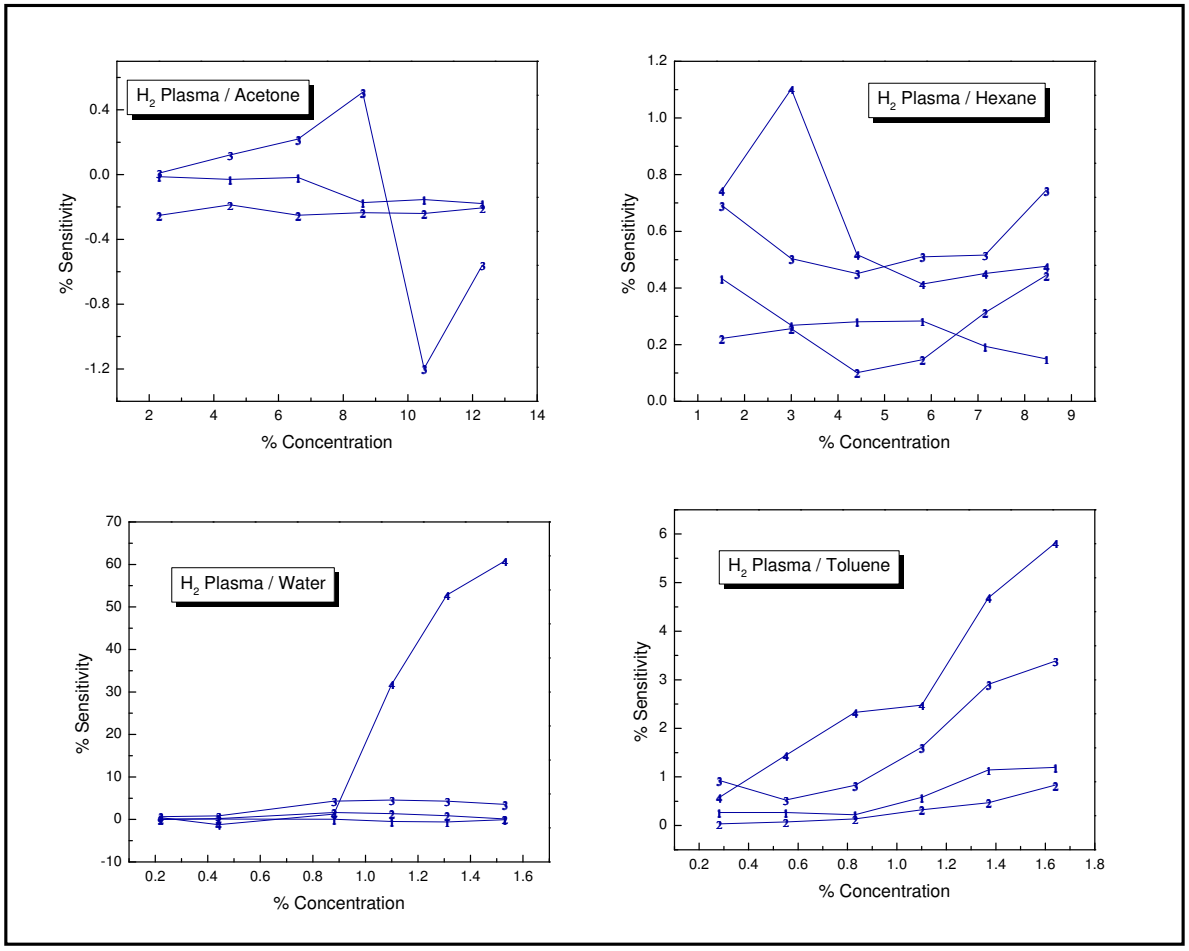

Fig. 3.22. Sensitivity of hydrogen plasma treated carbon films on diamond to the varying concentrations of different vapors: toluene, acetone, water and hexane. The number on data points indicates film type. P1 (~10^{-5} S), P2 (~10^{-6} S), P3 (~10^{-7} S), P4 (~10^{-8} S).

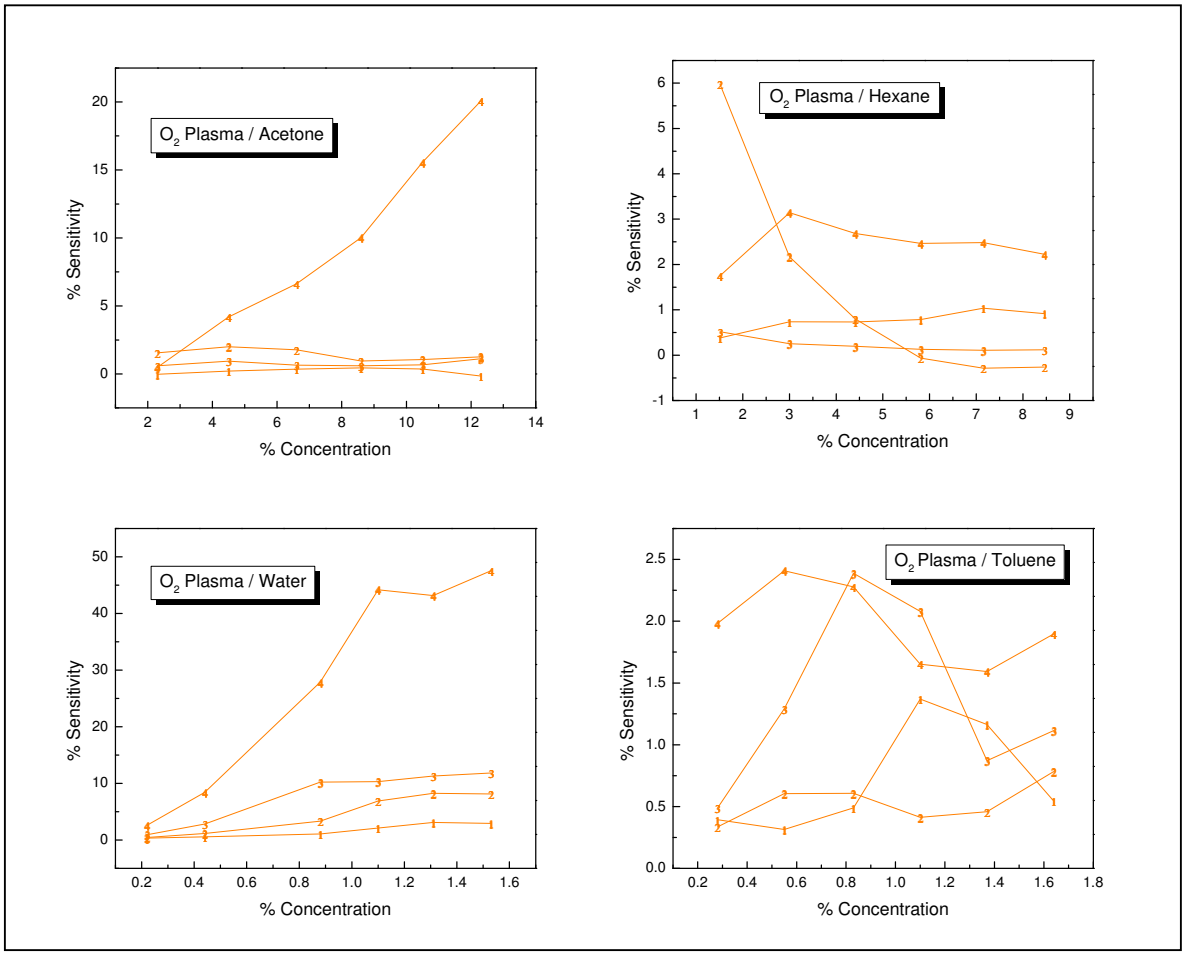

Fig. 3.23. Sensitivity of oxygen plasma treated carbon films on diamond to the varying concentrations of different vapors: toluene, acetone, water and hexane. The number on data points indicates film type. P1 (~10^{-5} S), P2 (~10^{-6} S), P3 (~10^{-7} S), P4 (~10^{-8} S).

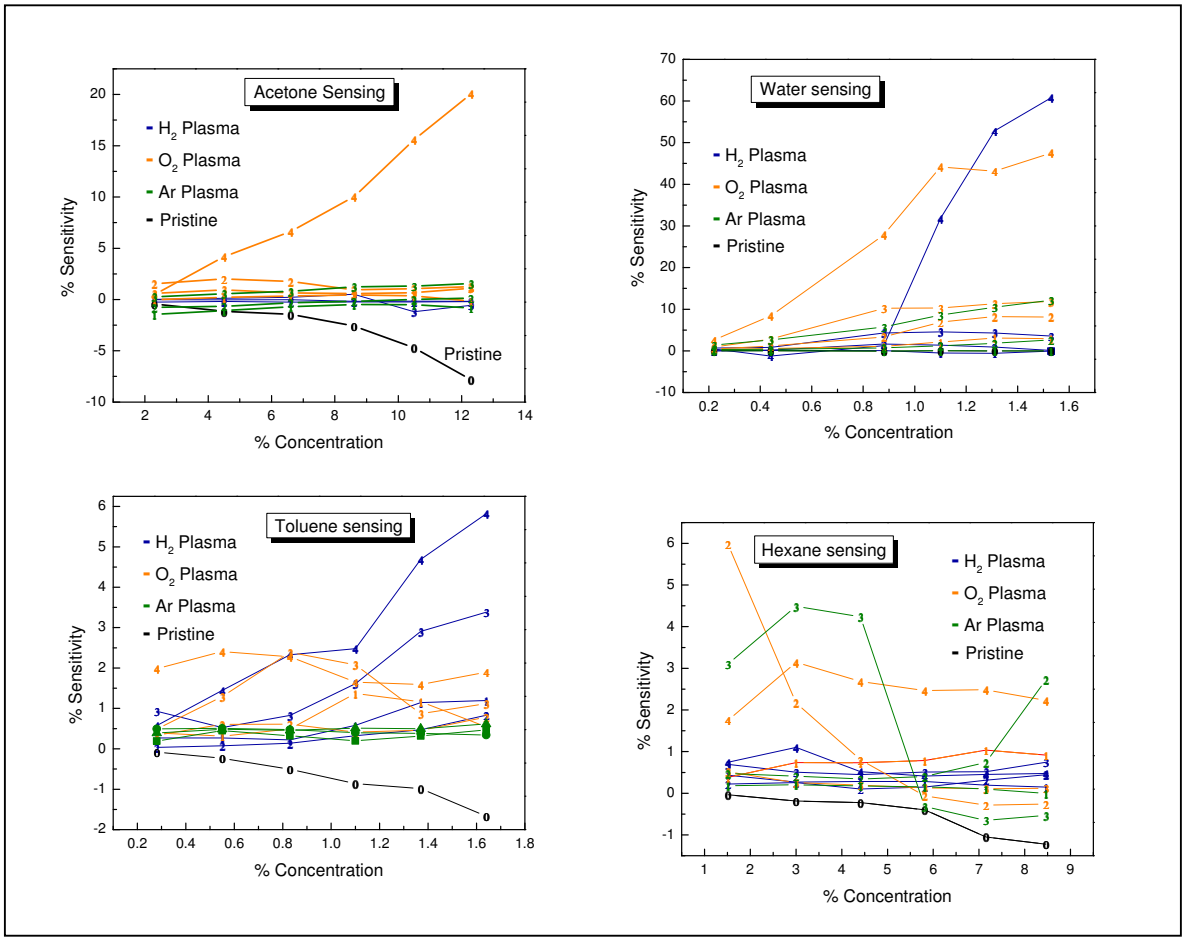

Fig. 3.24. The comparison of chemical sensitivities of hydrogen, oxygen, and argon plasma treated carbon films on diamond. The number and color of data points indicate film type and plasma type, respectively. P1 (~10^{-5} S), P2 (~10^{-6} S), P3 (~10^{-7} S), P4 (~10^{-8} S).

3.6.2 Model for chemical sensing

Unlike thermal sensitivity, which results from the thermal activation of the charge carriers, chemical sensitivity is based on chemical modulation in the conductance at the surface. Though, the exact mechanism of this effect is still not clear, obviously the conductance change starts with the adsorption of analyte molecules at the film's surface (Fig. 3.25). The sensitivity would then depend upon extent and nature of the molecular interaction with the film's surface. Observed higher response to water indicates greater interaction of water molecules with the surface probably through hydrogen bonding with surface sites containing groups like hydroxyl. On oxygen plasma etching (a known technique for modification of different carbon surfaces [190-195], additional adsorption sites may be introduced on the surface. This causes an increase in the number of interacting molecules and enhancement of sensitivity. The initial films, which do not have enough coverage of adsorption sites show almost constant sensitivity on increase in water vapor concentration. The behavior becomes increasingly exponential as the films are etched (Fig. 10c). In contrast, sensitivity to acetone, which does not form hydrogen bonds, is much lower. Also, unlike water, in case of acetone, exponential increase on increasing vapor concentration is not observed, at least for the intermediate plasma etched films (Fig. 10d).

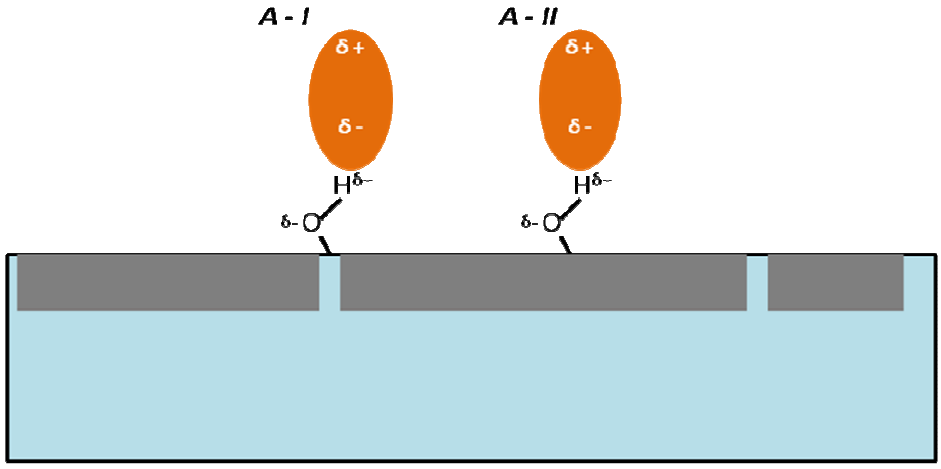

Fig. 3.25. Adsorption of dipolar molecules on a diamond surface containing plasma-etched carbon nanofilms. A-I: Adsorption at the bare diamond surface separating conductive carbon structures, A-II: Adsorption at the area containing conductive carbon.

We further propose that there are two ways in which the interacting molecules may modulate the surface conductance. Firstly, it may occur when the molecules adsorb on the diamond surface within the gaps separating the carbon nanoislands (A-I in Fig. 13). The adsorbed molecules can provide alternate conduction pathways or may facilitate tunneling through the energy barrier between the islands. Secondly, the molecules absorbed on the carbon nanofilm (A-II in Fig. 13) may change its electronic properties and in particular conductance. This could occur either by donor-acceptor charge transfer between the adsorbed molecules and the conductive surface or by the charge induction due to localized electric field near the adsorption site. Donor-acceptor charge transfers have been reported for semi-conducting carbon nanotubes [100, 196, 197]. The charge induction is an effect working in chemical field-effect transistors.

3.7 Conclusion

Conductive temperature/chemically sensitive carbon nanofilms can be obtained on diamond surface by annealing at temperatures above 1000 ºC in vacuum or inert gas atmosphere followed by plasma etching. These films consist essentially of amorphous carbon. Thickness, continuity and atomic structure of the films are strong factors of their sensitivity measured as the relative change of conductivity during the temperature change or exposure to chemical analytes. The temperature sensitivity of the films can be as high as an order of magnitude for a 100 ºC change in temperature. The as-grown carbon nanofilms on diamond show negative response (decrease in conductance) to the vapors of acetone, toluene and hexane, and positive response (increase in conductance) to the water vapor. Sensitivity to toluene is more than 4 times of that to acetone, which in turn is about 10 times of that to hexane. Plasma treatment changes the sensitivity to a positive value for all the organic vapors. The exposure to oxygen plasma renders the carbon nanofilms on diamond selectively sensitive to acetone and water, while, hydrogen plasma to that of toluene. Remarkably, along with the fast chemical response, the films exhibit fast recovery (1-2 min) even at high vapor concentrations. The different responses to different analytes imply that the carbon nanofilms are sensitive to the electronic structure of the absorbed molecules and as such may have a potential in their use as chemically selective sensors. It is important to note that the presented carbon-nanofilm-on-diamond sensing structures are all-carbon. Carbon and especially diamond are known for their bio-compatibility. Thus the demonstrated sensors may be of interest for the researchers working in the area of bio- and medical sensorics.

Chapter IV

Chemical Sensing Properties of Carbon Nanofilms on Quartz

4.1 Introduction

The type of bonding and structural order in carbon nanofilms have a significant effect on their electronic properties. In this regard, disordered carbon films and those obtained by thermal ordering at different temperatures model different carbon systems. The chapter discusses the chemical and temperture sensing properties of low-order carbon films, and the mechanism for charge conduction.

4.2 Raman spectroscopy

Fig. 4.1a shows Raman spectra of the as-deposited and annealed carbon films. The Raman intensity values are on an arbitrary scale, normalized with respect to 456 cm^{-1} Raman line of single crystalline quartz (substrate). A broad Raman band as expected for amorphous carbon is observed for the as-deposited film [185, 186, 198]. Two Raman peaks centered around 1350 cm^{-1}(D) and 1580 cm-^{1} (G) start evolving in the region 1200–1600 cm^{-1} on annealing and are more pronounced for temperatures above 600 ^{o}C.

In order to determine more accurate positions of the peaks, the Raman spectra of the films in the region 600–2000 cm^{-1} were fitted by two Gaussian functions, after subtracting the Raman spectrum of the substrate (Fig. 4.2). The as-deposited carbon film and those annealed at 400 ^{o}C and 1200 ^{o}C are shown for comparison.

The broad Raman band of the as-deposited carbon film consists of two peaks centered at 1287 and 1474 cm^{-1}. The peak at 1287 cm^{-1} first shifts to 1357 cm^{-1} on annealing at 400 ^{o}C

and then remains almost constant at 1320 cm^{-1} on increasing the annealing temperature (D peak). In contrast, the peak at 1474 cm^{-1} shifts to 1562 cm^{-1} on annealing at 400 ^{o}C and then gradually increases to around 1583-1585 cm^{-1} with an increase in annealing temperature to 1200 ^{o}C (G peak). This gradual increase in the G peak position and the almost constant D peak position keeps the gap between the two bands widening (Fig. 4.1b). Full width at half maximum (FWHM) for the G band decreased from about 250 cm^{-1} to a constant value of about 130 cm^{-1} (Fig. 4.3). Also, the ratio of areas under D and G bands (I_D/I_G), decreased after an initial increase at 400 ^{o}C.

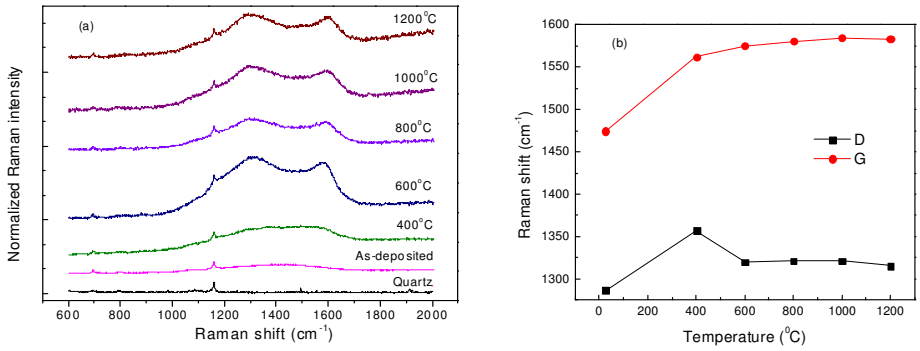

4.1 (a) Raman spectra of the as-deposited and annealed carbon films. Annealing temperatures are indicated on the side. Raman spectrum of the substrate (quartz) is also included for comparison. The scattering intensities are normalized with respect to the 456 cm^{-1} Raman line observed for the substrate. (b) Band positions (G, D) are measured from the simulated G and D bands, as functions of the annealing temperature.

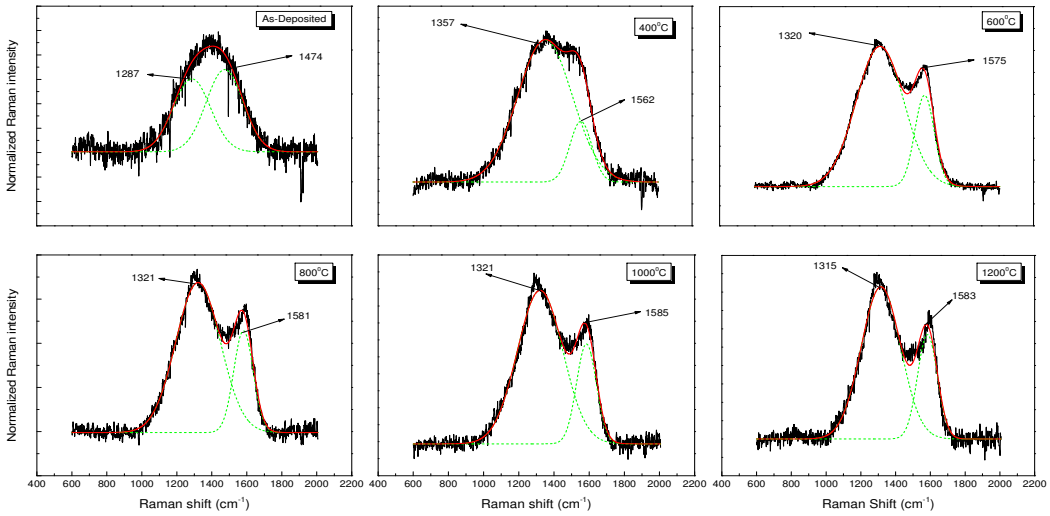

Fig. 4.2. Raman spectra of the as-deposited and annealed carbon film fitted by two Gaussian functions (dotted green curves) as simulated G and D bands in the spectral region 600–2000 cm^{-1}.The resultant fitted Raman spectra are shown by red curves.

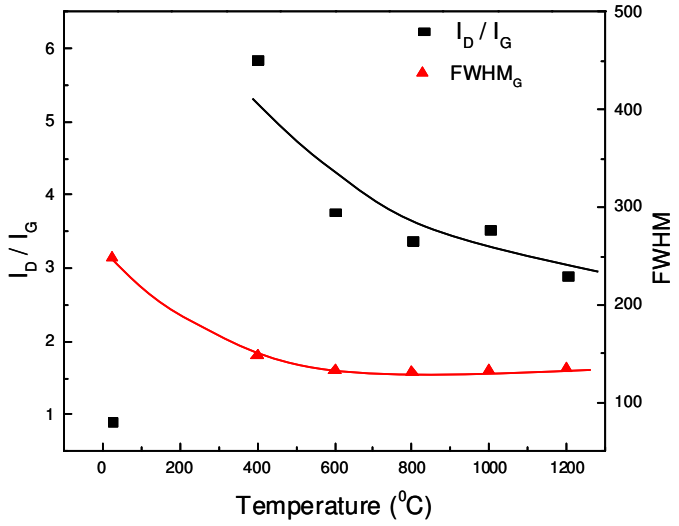

Fig. 4.3. Evolution of Raman intensity ratio of D and G bands (I_D/I_G) (black data curve, left axis), and full width at half maximum (FWHM) of G band (red data curve, right axis) with annealing temperature.

The shift of G band toward higher frequencies is in accordance with the hardening of corresponding Raman modes of vibration of sp^2 carbons on increase in graphitic domain size [185, 198]. In order to understand the observed trend in FWHM, it may be noted that a narrower distribution of energy of a vibrational mode should result in a smaller band width. Thus, for G scattering for which the vibrational energy is primarily determined by the size of the sp^2 cluster, the greater the disorder or range of sp^2 cluster sizes, the broader the band [185]. Therefore, the observed decrease in FWHM of G band on annealing and the shift toward higher frequencies indicate atomic ordering and a possible increase in graphitic domain size on heating. This is also supported by the observed decrease in intensity ratio of D and G Raman bands (I_D/I_G) with increase in annealing temperature. As previously shown for nanocrystalline graphite, the average crystallite size (L_a) is inversely proportional to the intensity ratio (I_D/I_G) and is given by the empirical relation [199]:

$$L_a, \text{nm} = 2.4 \times 10^{-10} \times (\lambda, \text{nm})^4 \times (I_D/I_G)^{-1} \qquad \text{Eq. 4.1}$$

where Raman excitation wavelength (λ) and calculated value of L_a are in nm.

The above equation can be used to estimate the average size of the graphitic domains in the annealed carbon films. The domain size, thus calculated, increased almost twice, from about 50 nm to about 100 nm on increasing the annealing temperature from 400 to 1200 ^{0}C. Eq. (4.1) may not apply to the as-deposited carbon film, which is made up of randomly sputtered carbon atoms on the substrate.

4.3 Electrical conductance and its dependence on temperature

The as-deposited carbon films were insulating and became increasingly conductive on annealing at high temperatures. Fig. 4.4a shows surface conductance of the as-deposited and annealed carbon films at their corresponding maximum temperatures. The as-deposited carbon films showed conductance of the order of 10^{-8} S. A sharp increase in conductance to about 8 x 10^{-5} S was observed on heating at 400 ^{o}C for 1 hr. The conductance increased steadily on further heating, attaining a value of about 10^{-3} S on annealing at 1200 ^{o}C. This may be related to the atomic ordering induced by heating as revealed by Raman measurements.

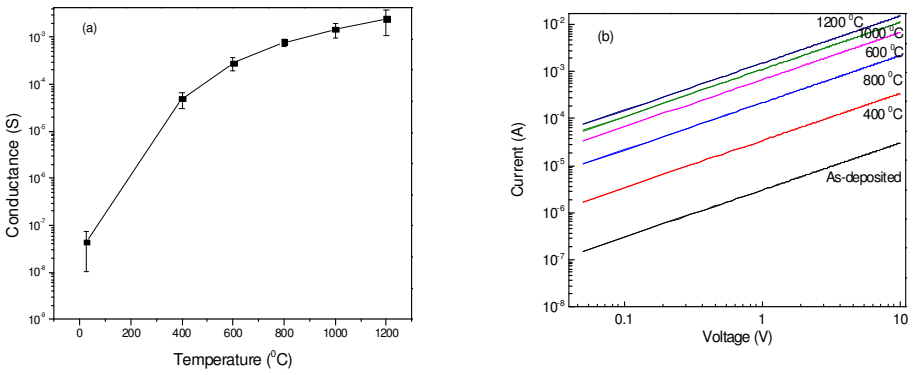

Fig. 4.4. (a) Dependence of the surface conductance on annealing temperature, and (b) Current-voltage characteristics of the as-deposited carbon film and films annealed at different annealing temperatures.

All the carbon films showed a steady and reversible increase in conductance with an increase in temperature when measured in the range from 20 to 300 ^{0}C. The observed thermally activated conductance closely fitted with a simple exponential dependence on temperature (Fig. 4.5a). The corresponding empirical relation is written in terms of temperature independent empirical constants A and B as:

$$G = A \exp (BT) \qquad \text{Eq. 4.2}$$

This is remarkably different from the commonly used model for the thermal activation of conductance via activation energy, following a T^{-1} dependence in the exponent as below.

$$G = G_0 \exp(-E_a/kT) \qquad \text{Eq. 4.3}$$

Where, G_0 is a constant independent of temperature, k is the Boltzmann's constant and E_a is the activation energy.

Instead, the films, especially the ones annealed at lower temperatures, deviated strongly from the activation energy model as indicated by the non-linearity of corresponding plots of lnG with T^{-1} (Fig. 4.6a). Formally, the average activation energy is calculated from the slope of lnG vs T^{-1} (Fig. 4.6b) and may approximate existing barriers to charge conduction discussed later. The observed sharp decrease in its value with annealing is in accordance with the structural ordering induced by heating.

Simulation was also done with respect to a variable-range hopping model of conductance often used for disordered systems and described by exponential dependence of conductance on $T^{-1/4}$ [187-189]. However, similar to the activation energy model, it too showed significant deviation for the films annealed at lower temperatures.

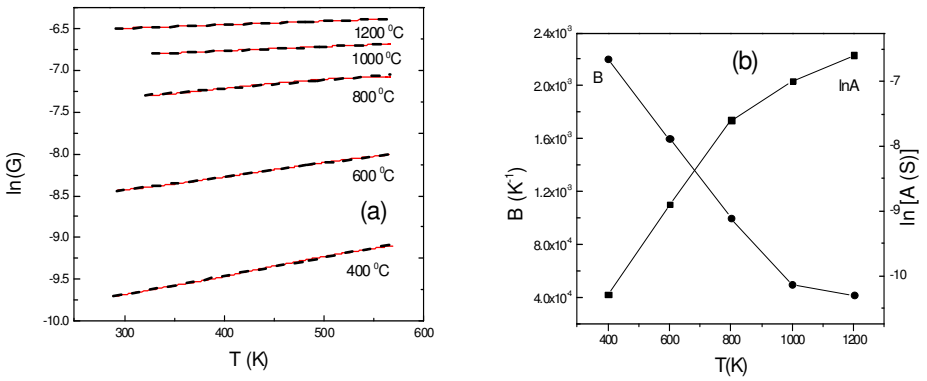

Fig. 4.5. (a) Logarithm of surface conductance as a function of T and corresponding best fit lines for carbon films annealed at different temperatures (as indicated). (b) Intercept (lnA) and slope (B) of the best-fit lines as functions of annealing temperature.

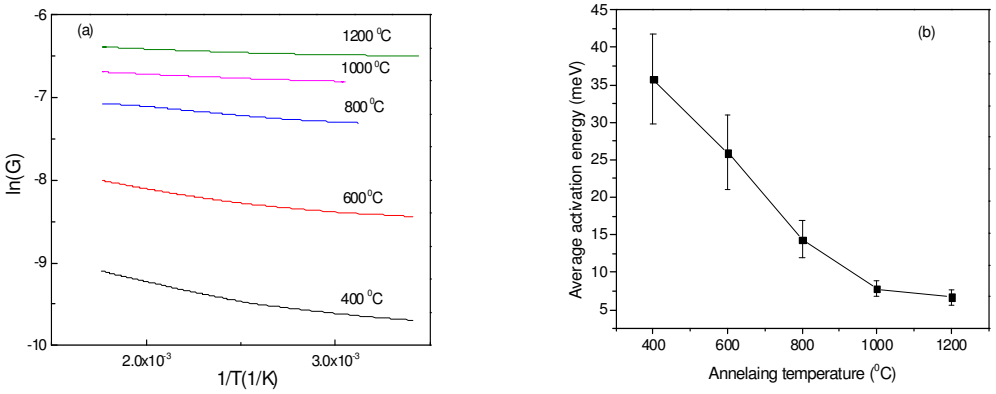

Fig. 4.6. (a) Logarithm of surface conductance as a function of T^{-1} for carbon films annealed at different temperatures (as indicated). (b) Dependence of the activation energy averaged over the heating range on annealing temperature. The corresponding standard deviation values are also included.

In pursuit of an alternate model of conductance that applied in the whole experimental range, we refer to some low conducting semiconductors [200] and organic solids [201], where a similar behavior was observed. The model was based on the tunneling of charge carriers through thermally vibrating energy barriers [200, 201] and described the observed simple exponential dependence of conductance on temperature. In the present case, main barriers to electrical conduction come from insulating domains. High activation energy as seen above is indicative of high barrier height. Thus, tunneling though the barriers may be more energetically favorable than hopping.

We examine the observed temperature dependence of conductance based on rectangular barriers as approximated by Simmons under low voltage bias [202]. The corresponding I–V relationship is:

$$I = \eta\,(2m\,\Delta E)^{1/2}\,e^{2}\,a/(\hbar^{2}d)\,\exp\left[-2\,\eta\,(2m\,\Delta E)^{1/2}/\hbar\,d\right]V \qquad \text{Eq. 4.4}$$

Where, m is the electronic mass, e is the electronic charge, a is the cross section area of the current flow, ΔE is the energy barrier, and d is the barrier width. η is a dimensionless factor introduced to account for the finite voltage bias and effective mass, and is 1 for zero bias.

As expected from Eq. (4.4), observed I–V characteristics are linear. Now, the assumption that barriers are under thermal vibrations may be applied to the above model. We consider the vibration to be simple harmonic with angular frequency ω and equilibrium width d_0, independent of temperature, and mass of the vibrating sites as m_s. Following the method used by Hurd [200], it may be easily shown that Eq. (4.4) reduces to:

$$I = A \exp [B\,T]\, V \qquad \text{Eq. 4.5}$$

$$A = \eta\, (2m\,\Delta E)^{1/2}\, e^2\, a / \hbar^2 d_0) \exp [-2\,\eta\, (2m\,\Delta E)^{1/2}\, d_0 / \hbar\,]$$

$$\mathbf{B} = 4\eta\, k\,\Delta E\, (m/m_s) / \hbar^2 \omega^2$$

The above temperature dependent I-V characteristic is same as the observed empirical relation between conductance (I/V) and temperature (Eq. 4.2).

For, ΔE ~30 meV (of the order of experimentally observed activation energy for film annealed at 400 ^oC), e ~10^{-19} C (electronic charge), m ~10^{-30} kg (electronic mass), d_0 ~10 nm (of the order of surface features), $\hbar\omega$ ~ k T (T ~ 300 K), m_s ~10^{-26} kg (atomic mass), a ~10^{-10} m^2 (thickness ~100 nm, width ~1 mm), η ~1 (bare electronic mass condition for simplicity); the resulting values are B ~10^{-6} K^{-1} and lnA ~ −12.

The experimental values of B and lnA, as slope and intercept of linear plots of lnG and T respectively, are plotted in Fig. 4.5b. B decreases steadily from 2.2 x 10^{-3} K^{-1} (film annealed at 400 ^oC) to 4.2 x 10^{-4} K^{-1} (film annealed at 1200 ^oC). In comparison, lnA increases steadily from −10.3 (film annealed at 400 ^oC) to -6.6 (film annealed at 1200 ^oC).

From Eq.4.5, observed decrease in B on annealing may be related to decrease in average barrier height ΔE resulting from the atomic ordering induced by heating. The ordering also decreased the average barrier width d_0 (size of insulating domains), which along with ΔE increased lnA.

Thus, the conductance model based on a thermally vibrating energy barrier is able to describe qualitatively the observed simple exponential dependence of conductance on

temperature. A better quantitative match would require a more accurate estimate of the barrier height ΔE, the size of the insulating domains (d_0), and mass of the graphitic domains (m_s).

4.4 Chemical Sensitivity

The response of the carbon films as the films are exposed to alternating cycles of diluted vapors of NO_2/NH_3 and pure dry nitrogen gas are shown separately for as-deposited (Fig. 4.7) and annealed films (Fig. 4.8). The response is shown as changing conductance values normalized with respect to the initial conductance in dry nitrogen and recorded versus time. It is seen that for annealed films conductance increases on exposure to NO_2 and decreases when exposed to NH_3, whereas, as-deposited films show an increase in conductance for both the analytes. In comparison, the sensitivity to water vapor when tested separately was negligible for all the films and hence the observed response may be considered solely due to the respective analyte molecules.

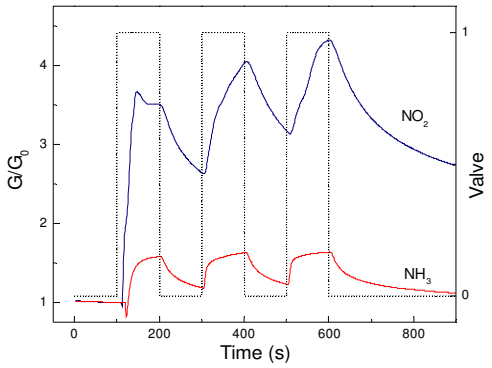

Fig. 4.7. Response of as-deposited carbon films for NH_3 and NO_2 vapors. The dotted curves are the exposure cycles with valve position (V3 in Fig. 2.3) on the right-vertical axis ('0' for flow of pure dry nitrogen gas, '1' for flow of the analyte vapors).

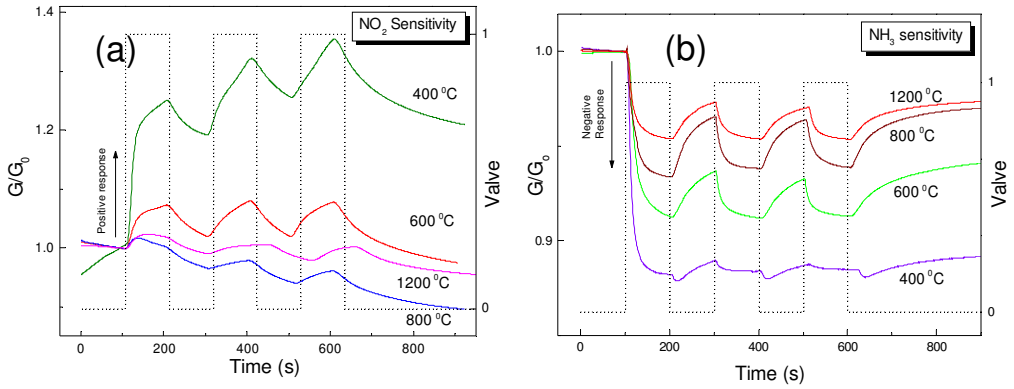

Fig. 4.8. Response of carbon films annealed at different temperatures (as indicated) for (a) NO_2 vapors, and (b) NH_3 vapors. The dotted curves are the exposure cycles with valve position (V3 in Fig. 2.3) on the right-vertical axis ('0' for flow of pure dry nitrogen gas, '1' for flow of diluted analyte vapors).

Further analysis of the response of the films showed an exponential dependence of conductance on exposure as fitted by the functions of the general form:

$$G/G_0 = \alpha - \beta \exp[-(t - t_o)/\tau] \qquad \text{Eq. 4.6}$$

Fig. 4.9 shows the fitted response curve to NO_2 for a sample carbon film. Fitting is done after an initial transit time (t_o), film takes for effective interaction with analyte molecules. τ may be easily identified as time constant of the response, while β is the maximum response if the exposure time is sufficiently large. α is the initial offset in conductance, α - β being close to 1. Thus, τ and β are the primary parameters of sensing and are characteristics of the films. β is related to the material property of the film and determines the total change in the conductance, if the film is exposed long enough to reach saturation. In comparison, τ is a characteristic response time and should be primarily determined by the surface features that facilitate interaction of analyte molecules with surface. The expression $\sigma = \beta/\tau$, which is the slope of the function G/G_o at t_o, determines the response of the film and is referred as sensitivity. Unlike, the more common expression of sensitivity as relative change in the conductance, $S = (G_t - G_o)/G_o$, where G_t is the conductance after a specified time and G_0 is the initial conductance, σ doesn't need a reference time. Also, S for a specific time may be easily calculated if σ and one of the two independent parameters β and τ are known.

Fig. 4.10 shows fitted curves and the corresponding characteristic parameters τ and β in the first exposure cycle. β for NH_3 is negative (negative response) and for NO_2 is positive (positive response). The sensitivity, $\sigma = \beta/\tau$ is plotted as a function of annealing temperature (Fig. 4.11). Overall, a decrease in sensitivity is observed on increasing the annealing temperature. Sensitivity of as-deposited film for NO_2 drops down by almost one tenth on annealing at 400 ^oC. The sensitivity continues to decrease steeply on increasing the annealing temperature. Approximately a two order of magnitude decrease is observed for a film

annealed at 1200 ^{o}C. Like NO_2, sensitivity for ammonia is positive in the beginning. However, it changes to a negative value on annealing at a temperature around 200 ^{o}C. The negative sensitivity shows a maximum at around 400 ^{o}C and decreases steadily thereafter. Film annealed at 1200 ^{o}C shows a negative sensitivity just about one third of the sensitivity of the film annealed at 400 ^{o}C.

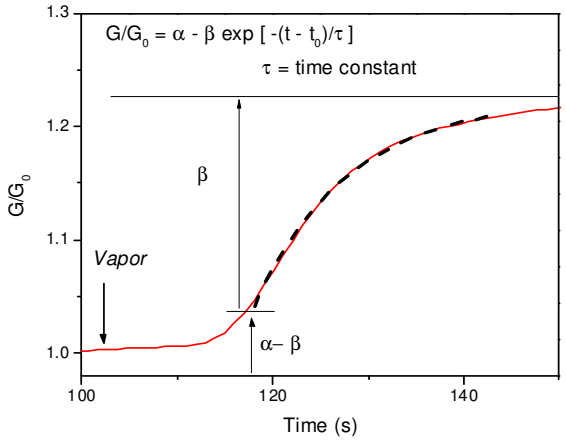

Fig. 4.9. Representative response curve to NO_2 of a sample annealed film fitted by an exponential function. The function and the meaning of its parameters α, β and τ are indicated on the plot.

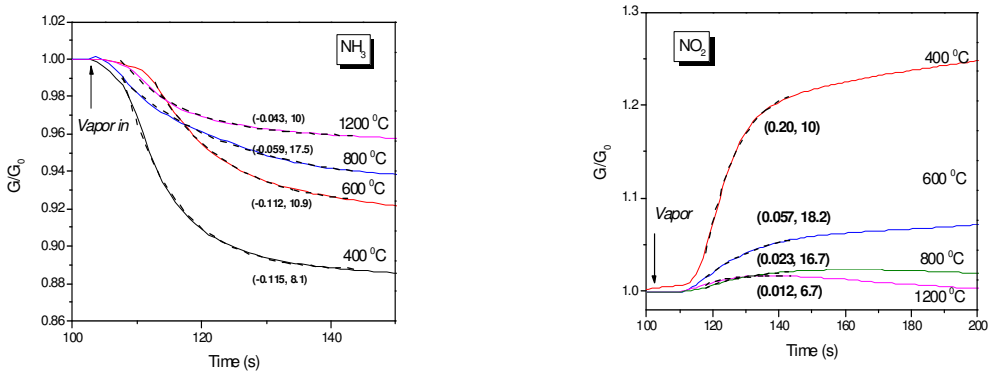

Fig. 4.10. Response curves of carbon films annealed at different temperatures (as indicated) to (a) NH_3, and (b) NO_2, as fitted by exponential functions. The values given in parentheses are the characteristic parameters β and τ, in order.

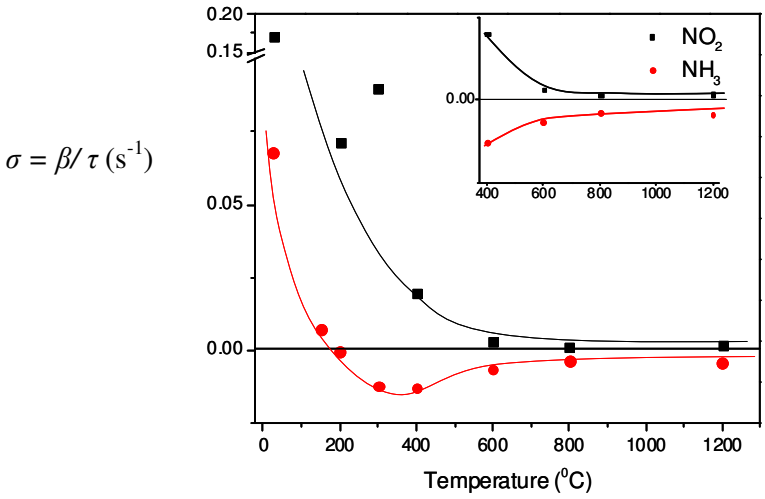

Fig. 4.11. Sensitivity, $\sigma = \beta/\tau$ of the carbon films to NO_2 and NH_3 vapors as the functions of annealing temperature. The inset highlights the opposite response of the films annealed at 400 ^{o}C or higher.

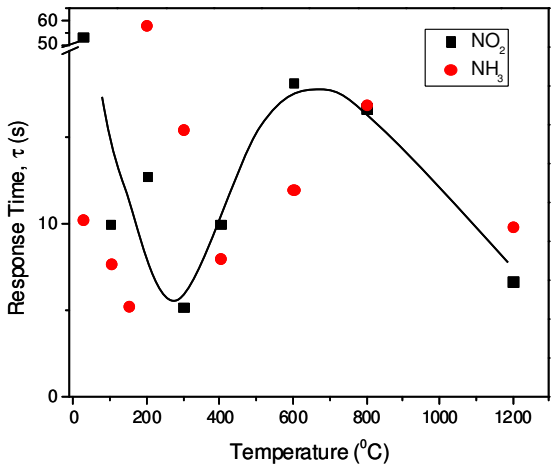

Fig. 4.12. Response time, τ of the carbon films to NO_2 and NH_3 vapors as the functions of annealing temperature. The curve shows the trend for NO_2. A similar trend is seen for NH_3.

The contrast in sensitivity toward NH_3 and NO_2 may be explained by the opposite donor-acceptor properties of the two molecules. Upon interaction with the surface they may change its electronic property differently by the charge transfer.

Qualitatively similar sensing behavior was observed for graphene [60, 61] and P-type single-walled CNTs [40, 80, 83, 88, 94]. They showed increases in resistance on exposure to ammonia and decreases when exposed to NO_2. It was reasoned that the change in resistance was due to the change in majority charge carrier density (holes). Injection of electrons by ammonia to the conduction band decreased the hole density and hence the increased resistance, whereas, NO_2 depleted the electrons from the surface, thereby increasing the hole concentration and decreasing the resistance. In the present case, it seems that carbon films are also of p-type and interaction with NH_3 causes a decrease in conductance and an increase with NO_2 for the same reason. Charge carrier density in the more ordered films obtained after high temperature annealing should be significantly greater and hence less sensitive to the

charge transfer at the surface. This explains the decrease in both negative and positive sensitivities with an increase in annealing temperature.

The opposite sign of sensitivity of as-deposited films compared to the annealed ones is probably of different origin. The as-deposited film consists largely of randomly sputtered carbon atoms, and charge transfer with the analyte molecules may not occur. Alternatively, adsorbed polar molecules may provide alternate conduction pathways and hence increase conductance. Interestingly, the films are insensitive to water vapors. This selective response to NH_3 and NO_2 vapors needs to be further studied. Annealing to a temperature above 200 ^oC, causes sufficient ordering in the film for charge transfer to be predominant. This results into usual negative response to NH_3 vapors as described before.

The response time is plotted as function of the annealing temperature (Fig. 4.12). The response time first decreased on annealing to 400 ^oC and increased thereafter, exhibiting maxima at a temperature around 700 ^oC for both the analytes. This indicates a faster response due to the increased per unit area adsorption of analyte molecules on the film, caused by rapid thermal ordering of randomly disordered carbon atoms. However, above 400 ^oC, where charge transfer is the predominant phenomenon, adsorption is assisted by the presence of other surface defects like the oxygen sites, through greater extent of hydrogen bonding with the analyte molecules. The decrease in defect density thus may lead to lower adsorption and hence slower response. On the other hand, an increased charge transfer rate due to increase in graphitic size will lead to faster response. It seems, the interplay of these two opposing factors results maxima in the response time, at an intermediate temperature around 700 ^oC.

4.5 Conclusions

Carbon films on quartz, reported herein exhibit chemical sensing characteristics similar to those of carbon nanotubes and graphenes. The decrease in their conductance on exposure to NH_3 and the increase on exposure to NO_2 vapors is observed. Temperature sensitivity, observed as simple exponential dependence on temperature, may be described using conductance model based on tunneling through thermally vibrating energy barriers. Such a behavior was also previously observed for some low-conducting semiconductors and organic solids. Both temperature and chemical sensitivity are directly related to atomic ordering in the film, induced by heating at high temperatures. The phenomenological description of the chemical sensing of the films may be given in terms of the time constant τ and the maximum relative change in conductance β when allowed to reach saturation. β is related to the material structure of the film, while, τ depends on the surface properties of the film. The expression, $\sigma = \beta/\tau$ may be considered as the measure of chemical sensitivity of the films. Sensitivities to both NH_3 and NO_2 vapors decrease in magnitude on increasing the annealing temperature. The possible mechanism may be based on the charge transfer with analyte molecules and the formation of additional conduction pathways upon interaction with the analyte molecules. The former is more predominant in the annealed films as indicated by the opposite response to the acceptor (NO_2) and donor molecules (NH_3). The positive response of as-deposited films to NH_3 vapors change to negative on annealing at a temperature around 200 ^{o}C.

Summary of the Major Results

1. The first in situ study of high temperature graphitization of diamond surface in inert atmosphere has been performed. It has been shown that the surface conductance of diamond increases continuously with temperature and becomes increasingly irreversible at temperatures above 1000 ^{o}C. Stable conductive films of thickness in the range 10 to 100 nm and specific resistivity 10^{-3} to 10^{-4} Ω.m have been obtained depending upon the heating conditions. A half-transparent thin film of high surface adhesion to the diamond surface is obtained by annealing in vacuum at a pressure below 10^{-4} mbar.
2. The exposure to plasma reduces the surface conductance of the carbon nanofilms on diamond as result of a partial removal of carbon and the plasma-stimulated amorphization. The rate of reduction of conductance and hence etching ability of plasma depends on its chemical composition, being most effective for hydrogen, followed by oxygen and argon, and ineffective for SF_6. At the initial stages of etching, the conductance of thick films drops linearly with etching time, and then reduces exponentially. The residual conductance remaining after prolonged plasma exposure is explained by the conductive carbon nano-islands trapped in the surface features of polished diamond surface. Thin films show an exponential drop of conductance from the very beginning of the etching. It has been shown that thin carbon nanofilms on diamond surface become increasingly amorphous with plasma exposure.
3. An alternate method of fabrication of carbon nanofilms on insulating substrates by carbon sputtering followed by high temperature annealing and plasma etching has been developed. It has been shown that the heating of as-sputtered carbon nanofilms on quartz substrates at temperatures over 400 ^{o}C results in an irreversible atomic ordering, considerable increase in conductivity, and lowering of the activation energy of

conductance. The maximum atomic ordering has been achieved at a temperature of 600 ^{o}C. At this temperature, the changes in conductance and activation energy are the highest. The thermal activation energy of conductance for the as-deposited carbon nanofilms is about 35 meV and it decreases to 5 meV after annealed at 1200 ^{o}C.

4. The carbon nanofilms on quartz and diamond, both exhibit an exponential dependence of their conductance on temperature. The temperature sensitivity of the nanofilms can be as high as an order of magnitude for a 100 ºC change in temperature. This behavior considerably deviates from the standard models based on the thermal activation of the charge carriers, or the variable range hopping. The experimentally observed exponential dependence of conductance G of the carbon nanofilms on temperature T can be well represented by a relation $G = \mathrm{A} \exp(\mathrm{B}T)$. This behavior is explained by a model based on the thermally vibrating energy barriers, which form between the carbon nanoclusters constituting the thin carbon nanofilms. The empirical constants A and B relate to the density of the carbon nanoclusters and the energy barrier height between them.
5. Along with temperature, the all studied carbon nanofilms exhibited considerable chemical sensitivity of their electrical conductance. The ratio $\sigma = \beta/\tau$ is proposed as a quantitative measure of the chemical sensitivity, where β is the maximum change in the conductance induced by the exposure to chemical analyte and τ is a characteristic time of this change. It has been shown that β and τ are the parameters responsible for the bulk and surface properties of the sensing nanofilm: β is determined by the total change in the conductance of the film terminated with analyte molecules, and τ is determined by the interaction of the film surface with the analyte molecules.
6. The as-grown carbon nanofilms on diamond show negative response (decrease in conductance) to the vapors of acetone, toluene and hexane, and positive response (increase in conductance) to the water vapor. Sensitivity to toluene is more than 4 times

of that to acetone, which in turn is about 10 times of that to hexane. Plasma treatment changes the sensitivity to a positive value for all the organic vapors. The exposure to oxygen plasma renders the carbon nanofilms on diamond selectively sensitive to acetone and water, while, hydrogen plasma to that of toluene.

7. The conductance of the carbon nanofilms on quartz has been found to be of p-type. These films show opposite response to NO_2 and NH_3 molecules. NO_2, a known electron acceptor increases the conductance, while NH_3, a known electron donor decreases it. The thermally induced atomic ordering in the nanofilms on quartz decreases the relative response of their conductance on chemical exposure, while increasing the total conductance. In contrast, plasma treatment reduces the conductance and makes films more sensitive. Hence optimal parameters of the annealing and/or plasma treatment should be chosen in order to achieve the maximum chemical sensitivity.

References

1. Bogue, R., *MEMS sensors: past, present and future.* Sensor Review, 2007. **27**(1): p. 13.
2. Joo, S. and R.B. Brown, *Chemical sensors with integrated electronics.* Chem. Rev., 2008. **108**: p. 638-651.
3. Arshak, K.M., E.; Lyons, G.M.; Harris, J.; Clifford, S., *A review of gas sensors employed in electronic nose applications* Sensor Review, 2004. **24**(2): p. 18.
4. Zaitsev, A.M., et al., *Diamond pressure and temperature sensors for high-pressure high-temperature applications.* Phys. Status Solidi A, 2001. **185**: p. 59-64.
5. Kumar, V., et al., *Formation of carbon nanofilms on diamond for all-carbon based temperature and chemical sensor application.* Carbon, 2011. **49**: p. 1385-1394.
6. Kumar, V. and A.M. Zaitsev, *Temperature and chemical sensitivity of carbon films on quartz.* Carbon, 2012 **Published Online**.
7. Zaitsev, A.M. and V. Kumar, *Carbon film based sensors*, USPTO, Editor 2011: USA.
8. Joo, S.B., R., *Chemical Sensors with Integrated Electronics.* Chem. Rev. , 2008. **108**: p. 14.
9. Gurbuz, Y., et al., *Current conduction mechanism and gas adsorption effects on device parameters of the Pt/SnOx/diamond gas sensor.* IEEE Trans. Electron Devices, 1999. **46**: p. 914-920.
10. Agui, L., P. Yanez-Sedeno, and J.M. Pingarron, *Role of carbon nanotubes in electroanalytical chemistry: a review.* Anal Chim Acta, 2008. **622**: p. 11-47.
11. Carlisle, J.A., *Diamond films: Precious biosensors.* Nat. Mater., 2004. **3**: p. 668-669.
12. Haertl, A., et al., *Protein-modified nanocrystalline diamond thin films for biosensor applications.* Nat. Mater., 2004. **3**: p. 736-742.

13. Lin, Y., et al., *Advances toward bioapplications of carbon nanotubes.* J. Mater. Chem., 2004. **14**: p. 527-541.

14. Liu, L., et al., *Highly sensitive biosensor based on bionanomultilayer with water-soluble multiwall carbon nanotubes for determination of phenolics.* Biosens. Bioelectron., 2008. **24**: p. 306-312.

15. Merkoci, A., et al., *New materials for electrochemical sensing VI: Carbon nanotubes.* TrAC, Trends Anal. Chem., 2005. **24**: p. 826-838.

16. Niculescu, M., et al., *Quinohemoprotein alcohol dehydrogenase-based reagentless amperometric biosensor for ethanol monitoring during wine fermentation.* Anal. Chim. Acta, 2002. **463**: p. 39-51.

17. Wang, J., M. Musameh, and Y. Lin, *Solubilization of carbon nanotubes by nafion toward the preparation of amperometric biosensors.* J. Am. Chem. Soc., 2003. **125**: p. 2408-2409.

18. Sberveglieri, G., *Recent developments in semiconducting thin-film gas sensors.* Sens. Actuators, B, 1995. **B23**: p. 103-9.

19. Gopel, W. and G. Reinhardt, *Metal oxide sensors: new devices through tailoring interfaces on the atomic scale.* Sens. Update, 1996. **1**: p. 47-120.

20. Tuller, H.L., *Review of electrical properties of metal oxides as applied to temperature and chemical sensing.* Sens. Actuators, 1983. **4**: p. 679-88.

21. Bai, H. and G. Shi, *Gas sensors based on conducting polymers.* Sensors, 2007. **7**: p. 267-307.

22. Kang, M. and H.Y. Woo, *Conjugated polymers for sensor applications.* Kobunja Kwahak Kwa Kisul, 2009. **20**: p. 320-327.

23. Lantada, A.D. and P.L. Morgado. *Electroactive polymers as sensors for biodevices*. 2012. Pan Stanford Publishing Pte. Ltd.

24. Levine, M. and T.M. Swager. *Conjugated polymer sensors: design, principles, and biological applications*. 2011. Wiley-VCH Verlag GmbH & Co. KGaA.

25. Liu, C., *Recent developments in polymer MEMS.* Adv. Mater., 2007. **19**: p. 3783-3790.

26. Lonergan, M.C., et al., *Array-based vapor sensing using chemically sensitive, carbon black-polymer resistors.* Chem. Mater., 1996. **8**: p. 2298-2312.

27. Matsuguchi, M., *Polymer sensors.* Chem. Sens., 2008. **24**: p. 26-30.

28. Shimizu, K.D. and C.J. Stephenson, *Molecularly imprinted polymer sensor arrays.* Curr. Opin. Chem. Biol., 2010. **14**: p. 743-750.

29. Zhu, C., et al., *Conjugated polymers for sensitive chemical sensors.* Huaxue Jinzhan, 2011. **23**: p. 1993-2002.

30. Cantalini, C., et al., *Carbon nanotubes as new materials for gas sensing applications.* J. Eur. Ceram. Soc., 2004. **24**: p. 1405-1408.

31. Chopra, S., et al., *Selective gas detection using a carbon nanotube sensor.* Appl. Phys. Lett., 2003. **83**: p. 2280-2282.

32. Li, J., et al., *Carbon Nanotube Sensors for Gas and Organic Vapor Detection.* Nano Lett., 2003. **3**: p. 929-933.

33. Varghese, O.K., et al., *Gas sensing characteristics of multi-wall carbon nanotubes.* Sens. Actuators, B, 2001. **B81**: p. 32-41.

34. Wang, Y. and J.T.W. Yeow, *A review of carbon nanotubes-based gas sensors.* J. Sens., 2009: p. No pp. given.

35. Abraham, J.K., et al., *A compact wireless gas sensor using a carbon nanotube/PMMA thin film chemiresistor.* Smart Mater. Struct., 2004. **13**: p. 1045-1049.

36. Chen, H.-W., et al., *The application of CNT/Nafion composite material to low humidity sensing measurement.* Sens. Actuators, B, 2005. **B104**: p. 80-84.

37. Chen, S.G., et al., *Gas sensitivity of carbon black/waterborne polyurethane composites.* Carbon, 2004. **42**: p. 645-651.

38. Sayago, I., et al., *New sensitive layers for surface acoustic wave gas sensors based on polymer and carbon nanotube composites.* Procedia Engineering, 2011. **25**: p. 4.

39. Sljukic, B., et al., *Electrochemically polymerised composites of multi-walled carbon nanotubes and poly(vinylferrocene) and their use as modified electrodes: Application to glucose sensing.* Analyst, 2006. **131**: p. 670-677.

40. Kong, J., et al., *Nanotube molecular wires as chemical sensors.* Science, 2000. **287**: p. 622-625.

41. Penza, M., F. Antolini, and M.V. Antisari, *Carbon nanotubes as SAW chemical sensors materials.* Sens. Actuators, B, 2004. **B100**: p. 47-59.

42. Penza, M., et al., *Alcohol detection using carbon nanotubes acoustic and optical sensors.* Appl. Phys. Lett., 2004. **85**: p. 2379-2381.

43. Cahen, D., R. Naaman, and Z. Vager, *The cooperative molecular field effect.* Adv. Funct. Mater., 2005. **15**: p. 1571-1578.

44. Schoening, M.J., *"Playing around" with field-effect sensors on the basis of EIS structures, LAPS and ISFETs.* Sensors, 2005. **5**: p. 126-138.

45. Zhang, T., et al., *Electrochemically functionalized single-walled carbon nanotube gas sensor.* Electroanalysis, 2006. **18**: p. 1153-1158.

46. Darbari, S., Y. Abdi, and S. Mohajerzadeh, *A novel carbon-nanotube gas sensor based on field ionization from branched nanostructures.* Eur. Phys. J.: Appl. Phys., 2010. **52**: p. 30602/1-30602/5.

47. Hou, Z., et al., *A MEMS-based ionizations gas sensor using carbon nanotubes.* IEEE Trans. Electron Devices, 2007. **54**: p. 1545-1548.

48. Huang, B.-R., et al., *Gas ionization sensors with carbon nanotube/nickel field emitters.* J. Nanosci. Nanotechnol., 2011. **11**: p. 10849-10853.

49. Kermany, A.R., N.M. Mohamed, and B. Singh, *Characterization of aligned MWCNTs array as the sensing element for ionization gas sensor.* J. Appl. Sci., 2011. **11**: p. 1243-1248.

50. Modi, A., et al., *Miniaturized gas ionization sensors using carbon nanotubes.* Nature, 2003. **424**: p. 171-174.

51. Nikfarjam, A., et al., *Fabrication of gas ionization sensor using carbon nanotube arrays grown on porous silicon substrate.* Sens. Actuators, A, 2010. **A162**: p. 24-28.

52. Zhang, Y., J. Liu, and C. Zhu, *Novel gas ionization sensors using carbon nanotubes.* Sens. Lett., 2010. **8**: p. 219-227.

53. Kroto, H.W., et al., *C60: buckminsterfullerene.* Nature, 1985. **318**: p. 162-3.

54. Iijima, S., *Helical microtubules of graphitic carbon.* Nature, 1991. **354**: p. 56-8.

55. Odom, T.W., et al. *Atomic structure and electronic properties of single-walled carbon nanotubes*. 1998. American Chemical Society.

56. Tanaka, K., et al., *Electronic properties of carbon nanotube.* Chem. Phys. Lett., 1994. **223**: p. 65-8.

57. Bredas, J.L. and G.B. Street, *Electronic properties of amorphous carbon films.* J. Phys. C, 1985. **18**: p. L651-L655.

58. Frauenheim, T., et al., *Structure and electronic properties of amorphous carbon: from semimetallic to insulating behavior.* J. Non-Cryst. Solids, 1995. **182**: p. 186-97.

59. Kumari, L., V. Prasad, and S.V. Subramanyam, *Effect of iodine incorporation on the electrical properties of amorphous conducting carbon films.* Carbon, 2003. **41**: p. 1841-1846.

60. Dan, Y., et al., *Intrinsic Response of Graphene Vapor Sensors.* Nano Lett., 2009. **9**: p. 1472-1475.

61. Fowler, J.D., et al., *Practical Chemical Sensors from Chemically Derived Graphene.* ACS Nano, 2009. **3**: p. 301-306.

62. Dai, L., *Carbon nanotubes and related structures-new materials for the twenty-first century. By Peter J. F. Harris.* Chemphyschem, 2002. **3**: p. 463-464.

63. Thess, A., et al., *Crystalline ropes of metallic carbon nanotubes.* Science (Washington, D. C.), 1996. **273**: p. 483-487.

64. Wang, Y., et al., *Periodicity and alignment of large-scale carbon nanotubes arrays.* Appl. Phys. Lett., 2004. **85**: p. 4741-4743.

65. Wong, S.S., et al., *Carbon Nanotube Tips: High-Resolution Probes for Imaging Biological Systems.* J. Am. Chem. Soc., 1998. **120**: p. 603-604.

66. Dillon, A.C. and M.J. Heben, *Hydrogen storage using carbon adsorbents: past, present and future.* Appl. Phys. A: Mater. Sci. Process., 2001. **72**: p. 133-142.

67. Gooding, J.J., et al., *Protein electrochemistry using aligned carbon nanotube arrays.* J. Am. Chem. Soc., 2003. **125**: p. 9006-9007.

68. Xu, Q. and S.-F. Wang, *Electrocatalytic Oxidation and Direct Determination of L-Tyrosine by Square Wave Voltammetry at Multi-wall Carbon Nanotubes Modified Glassy Carbon Electrodes.* Microchim. Acta, 2005. **151**: p. 47-52.

69. Wong, E.W., P.E. Sheehan, and C.M. Lieber, *Nanobeam mechanics: elasticity, strength, and toughness of nanorods and nanotubes.* Science, 1997. **277**: p. 1971-1975.

70. Journet, C. and P. Bernier, *Production of carbon nanotubes.* Appl. Phys. A: Mater. Sci. Process., 1998. **67**: p. 1-9.

71. S.Ijima, *Helical microtubules of graphitic carbon.* Nature, 1991. **354**.

72. Vairavapandian, D., P. Vichchulada, and M.D. Lay, *Preparation and modification of carbon nanotubes: Review of recent advances and applications in catalysis and sensing*. Anal. Chim. Acta, 2008. **626**: p. 119-129.

73. Journet, C., et al., *Large-scale production of single-walled carbon nanotubes by the electric-arc technique.* Nature, 1997. **388**: p. 756-758.

74. Paladugu, M.C., et al., *Synthesis of carbon nanotubes by arc discharge in open air.* J. Nanosci. Nanotechnol., 2005. **5**: p. 747-752.

75. Zhu, H.-W., et al., *Synthesis of High Quality Single-Walled Carbon Nanotube Silks by the Arc Discharge Technique.* J. Phys. Chem. B, 2003. **107**: p. 6514-6518.

76. Scott, C.D., et al., *Growth mechanisms for single-wall carbon nanotubes in a laser-ablation process.* Appl. Phys. A: Mater. Sci. Process., 2001. **72**: p. 573-580.

77. Takahashi, S., et al., *Synthesis and characterization of carbon nanotubes grown on carbon particles by using high vacuum laser ablation.* Shinku, 2002. **45**: p. 609-612.

78. Pradhan, B.K., et al. *CVD synthesis of single wall carbon nanotubes*. 2002. American Chemical Society.

79. Cantalini, C., et al., *Sensitivity to NO2 and cross-sensitivity analysis to NH3, ethanol and humidity of carbon nanotubes thin film prepared by PECVD.* Sens. Actuators, B, 2003. **B95**: p. 195-202.

80. Cantalini, C., et al., *NO2 gas sensitivity of carbon nanotubes obtained by plasma enhanced chemical vapor deposition.* Sens. Actuators, B, 2003. **B93**: p. 333-337.

81. Cao, Q. and J.A. Rogers, *Ultrathin films of single-walled carbon nanotubes for electronics and sensors: a review of fundamental and applied aspects.* Adv. Mater., 2009. **21**: p. 29-53.

82. Celorrio, V., et al., *Electrochemical performance of Pd and Au-Pd core-shell nanoparticles on surface tailored carbon black as catalyst support.* Int. J. Hydrogen Energy: p. Ahead of Print.

83. Chopra, S., et al., *Carbon-nanotube-based resonant-circuit sensor for ammonia.* Appl. Phys. Lett., 2002. **80**: p. 4632-4634.

84. Collins, P.G., et al., *Extreme oxygen sensitivity of electronic properties of carbon nanotubes.* Science, 2000. **287**: p. 1801-1804.

85. Gao, X., et al., *Ammonia sensitivity of amorphous carbon film/silicon heterojunctions.* Appl. Phys. Lett., 2007. **91**: p. 122110/1-122110/3.

86. Goyal, R.N., et al., *Voltammetric determination of bisoprolol fumarate in pharmaceutical formulations and urine using single-wall carbon nanotubes modified glassy carbon electrode.* Electrochim. Acta, 2008. **53**: p. 2802-2808.

87. He, J.-B., C.-L. Chen, and J.-H. Liu, *Study of multi-wall carbon nanotubes self-assembled electrode and its application to the determination of carbon monoxide.* Sens. Actuators, B, 2004. **B99**: p. 1-5.

88. Li, Y.H., et al., *Mechanical and NH3 sensing properties of long multi-walled carbon nanotube ropes.* Carbon, 2006. **44**: p. 1821-1825.

89. Salimi, A., et al., *Simultaneous determination of ranitidine and metronidazole at glassy carbon electrode modified with single wall carbon nanotubes.* Electroanalysis, 2007. **19**: p. 1668-1676.

90. Valentini, L., et al., *Role of defects on the gas sensing properties of carbon nanotubes thin films: experiment and theory.* Chem. Phys. Lett., 2004. **387**: p. 356-361.

91. Wang, J., A.-N. Kawde, and M. Musameh, *Carbon-nanotube-modified glassy carbon electrodes for amplified label-free electrochemical detection of DNA hybridization.* Analyst, 2003. **128**: p. 912-916.

92. Wong, S.S., et al., *Covalently functionalized nanotubes as nanometer-sized probes in chemistry and biology.* Nature, 1998. **394**: p. 52-55.

93. Wong, Y.M., et al., *A novel microelectronic gas sensor utilizing carbon nanotubes for hydrogen gas detection.* Sens. Actuators, B, 2003. **B93**: p. 327-332.

94. Kauffman, D.R. and A. Star, *Carbon nanotube gas and vapor sensors.* Angew. Chem., Int. Ed., 2008. **47**: p. 6550-6570.

95. Nakashima, N., et al., *DNA dissolves single-walled carbon nanotubes in water. [Erratum to document cited in CA139:186348].* Chem. Lett., 2003. **32**: p. 782.

96. Wong, S.S., et al., *Functionalization of carbon nanotube AFM probes using tip-activated gases.* Chem. Phys. Lett., 1999. **306**: p. 219-225.

97. Zheng, M., et al., *DNA-assisted dispersion and separation of carbon nanotubes.* Nat. Mater., 2003. **2**: p. 338-342.

98. Mu, S.-c., et al., *Hydrogen storage in carbon nanotubes modified by microwave plasma etching and Pd decoration.* Carbon, 2006. **44**: p. 762-767.

99. Valentini, L., et al., *Sensors for sub-ppm NO2 gas detection based on carbon nanotube thin films.* Appl. Phys. Lett., 2003. **82**: p. 961-963.

100. Someya, T., et al., *Alcohol Vapor Sensors Based on Single-Walled Carbon Nanotube Field Effect Transistors.* Nano Lett., 2003. **3**: p. 877-881.

101. Staii, C., et al., *DNA-Decorated Carbon Nanotubes for Chemical Sensing.* Nano Lett., 2005. **5**: p. 1774-1778.

102. Sotiropoulou, S. and N.A. Chaniotakis, *Carbon nanotube array-based biosensor.* Anal. Bioanal. Chem., 2003. **375**: p. 103-105.

103. Sumanasekera, G.U., et al., *Thermoelectric chemical sensor based on single wall carbon nanotubes.* Mol. Cryst. Liq. Cryst. Sci. Technol., Sect. A, 2002. **387**: p. 31-37.

104. Wisitsoraat, A., et al., *Electron beam evaporated carbon nanotube dispersed SnO2 thin film gas sensor.* J. Electroceram., 2006. **17**: p. 45-49.

105. Carrero-Sanchez, J.C., et al., *Biocompatibility and Toxicological Studies of Carbon Nanotubes Doped with Nitrogen.* Nano Lett., 2006. **6**: p. 1609-1616.

106. Foldvari, M. and M. Bagonluri, *Carbon nanotubes as functional excipients for nanomedicines: II. Drug delivery and biocompatibility issues.* Nanomedicine, 2008. **4**(.): p. 183-200.

107. Kaiser, J.P., et al., *Carbon nanotubes - curse or blessing*. Curr. Med. Chem., 2011. **18**: p. 2115-2128.

108. Lam, C.-w., et al., *A Review of Carbon Nanotube Toxicity and Assessment of Potential Occupational and Environmental Health Risks.* Crit. Rev. Toxicol., 2006. **36**: p. 189-217.

109. Liopo, A.V., et al., *Biocompatibility of native and functionalized single-walled carbon nanotubes for neuronal interface.* J. Nanosci. Nanotechnol., 2006. **6**: p. 1365-1374.

110. Moench, I., et al., *Synthesis and characteristics of Fe-filled multi-walled carbon nanotubes for biomedical application.* J. Phys.: Conf. Ser., 2007. **61**: p. 820-824.

111. Morozan, A., et al., *The biocompatibility microorganisms-carbon nanostructures for applications in microbial fuel cells.* Phys. Status Solidi A, 2007. **204**: p. 1797-1803.

112. Nayagam, D.A.X., et al., *Biocompatibility of Immobilized Aligned Carbon Nanotubes.* Small, 2011. **7**: p. 1035-1042.

113. Popov, A.M., et al., *Biocompatibility and applications of carbon nanotubes in medical nanorobots.* Int. J. Nanomed., 2007. **2**: p. 361-372.

114. Smart, S.K., et al., *The biocompatibility of carbon nanotubes.* Carbon, 2006. **44**: p. 1034-1047.

115. Yokoyama, A., *Biological behavior of carbon nanotubes.* Baiomateriaru, 2006. **24**: p. 324-332.

116. Landstrass, M.I. and K.V. Ravi, *Resistivity of chemical vapor deposited diamond films.* Appl. Phys. Lett., 1989. **55**: p. 975-7.

117. Maier, F., et al., *Origin of Surface Conductivity in Diamond.* Phys. Rev. Lett., 2000. **85**: p. 3472-3475.

118. Davidson, J.L., et al., *Diamond as an active sensor material.* Diamond Relat. Mater., 1999. **8**: p. 1741-1747.

119. Gurbuz, Y., et al., *Analyzing the mechanism of hydrogen adsorption effects on diamond based MIS hydrogen sensors.* Sens. Actuators, B, 1996. **B35**: p. 68-72.

120. Gurbuz, Y., et al., *Integration of diamond film with metal-oxide electrode for gas sensor applications.* Proc. - Electrochem. Soc., 1997. **97-19**: p. 896-905.

121. Gurbuz, Y., et al., *Diamond microelectronic gas sensors.* Sens. Actuators, B, 1996. **B33**: p. 100-104.

122. Kang, W.P., et al., *CVD diamond sensing devices (invited).* Proc. - Electrochem. Soc., 2004. **2004-09**: p. 220-236.

123. Kang, W.P., et al., *A polycrystalline diamond thin-film-based hydrogen sensor.* Sens. Actuators, B, 1995. **B25**: p. 421-5.

124. Gurbuz, Y., et al., *Diamond microelectronic gas sensor for detection of benzene and toluene.* Sens. Actuators, B, 2004. **B99**: p. 207-215.

125. Robertson, J., *Diamond-like carbon.* Pure Appl. Chem., 1994. **66**: p. 1789-96.

126. Robertson, J., *Diamond-like amorphous carbon.* Mater. Sci. Eng., R, 2002. **R37**: p. 129-281.

127. Dearnaley, G. and J.H. Arps, *Biomedical applications of diamond-like carbon (DLC) coatings: A review.* Surf. Coat. Technol., 2005. **200**: p. 2518-2524.

128. Erdemir, A. and C. Donnet, *Tribology of diamond-like carbon films: recent progress and future prospects.* J. Phys. D: Appl. Phys., 2006. **39**: p. R311-R327.

129. Hainsworth, S.V. and N.J. Uhure, *Diamond like carbon coatings for tribology: production techniques, characterisation methods and applications.* Int. Mater. Rev., 2007. **52**: p. 153-174.

130. Luo, J.K., et al., *Diamond and diamond-like carbon MEMS.* J. Micromech. Microeng., 2007. **17**: p. S147-S163.

131. Kim, J.-I., A. Bordeanu, and J.-C. Pyun, *Diamond-like carbon (DLC) microelectrode for electrochemical ELISA.* Biosens Bioelectron, 2009. **24**: p. 1394-8.

132. Maalouf, R., et al., *Characterization of different diamond-like carbon electrodes for biosensor design.* Talanta, 2007. **72**: p. 310-314.

133. Morrison, M.L., et al., *Electrochemical and antimicrobial properties of diamond-like carbon-metal composite films.* Diamond Relat. Mater., 2006. **15**: p. 138-146.

134. Narayan, R.J., *Nanostructured diamondlike carbon thin films for medical applications.* Mater. Sci. Eng., C, 2005. **C25**: p. 405-416.

135. Celorrio, V., et al., *Electrochemical performance of Pd and Au-Pd core-shell nanoparticles on surface tailored carbon black as catalyst support.* Int. J. Hydrogen Energy, 2012. **37**: p. 7152-7160.

136. Kumar, V., et al. *Carbon nanofilms on diamond for gas and temperature sensing applications*. 2010. American Chemical Society.

137. Lukaszewicz, J.P., *An application of carbon-type semiconductors for the construction of a humidity-sensitive diode.* Sens. Actuators, B, 1992. **B6**: p. 61-5.

138. Lukaszewicz, J.P., *Carbon-film-based humidity sensor containing sodium or potassium. Recovery effect.* Sens. Actuators, B, 1999. **B60**: p. 184-190.

139. Lukaszewicz, J.P., M. Panas, and J. Siedlewski, *Sodium-doped carbon films for humidity sensor construction.* Sens. Actuators, B, 1996. **B32**: p. 221-226.

140. Lukaszewicz, J.P. and M. Skompska, *A novel carbon-based ionic conductor for humidity sensors.* Sens. Actuators, B, 2006. **B113**: p. 970-977.

141. Davies, G. and T. Evans, *Graphitization of diamond at zero pressure and at a high pressure.* Proc. Roy. Soc., Ser. A, 1972. **328**: p. 413-27.

142. Evans T., J.P.F., *A study of the transformation of diamond to graphite.* Proc. R. Soc. Lond. A 1964. **277**(1369): p. 10.

143. Haines, S.R., et al., *The initial stages of graphite formation on the diamond (100) 2 × 1 surface.* J. Electron Spectrosc. Relat. Phenom., 2006. **152**: p. 33-36.

144. Allen, M., B. Myer, and N. Rushton, *In vitro and in vivo investigations into the biocompatibility of diamond-like carbon (DLC) coatings for orthopedic applications.* J. Biomed. Mater. Res., 2001. **58**: p. 319-328.

145. Cheng, G., et al., *Biocompatibility between tissue-engineering diamond-like carbon film and human vascular endothelial cells.* Zhongguo Zuzhi Gongcheng Yanjiu Yu Linchuang Kangfu, 2009. **13**: p. 566-570.

146. Salgueiredo, E., et al., *Biocompatibility evaluation of DLC-coated Si3N4 substrates for biomedical applications.* Diamond Relat. Mater., 2008. **17**: p. 878-881.

147. Steffen, H.J., J. Schmidt, and A. Gonzalez-Elipe, *Biocompatible surfaces by immobilization of heparin on diamond-like carbon films deposited on various substrates.* Surf. Interface Anal., 2000. **29**: p. 386-391.

148. Uzumaki, E.T., et al., *Biocompatibility of titanium based implants with diamond-like carbon coatings produced by plasma immersion ion implantation and deposition.* Key Eng. Mater., 2008. **361-363**: p. 677-680.

149. Vaijayanthimala, V., et al., *The biocompatibility of fluorescent nanodiamonds and their mechanism of cellular uptake.* Nanotechnology, 2009. **20**: p. 425103/1-425103/9.

150. Yang, P., et al., *Structure and properties of annealed amorphous hydrogenated carbon (a-C:H) films for biomedical applications.* Surf. Coat. Technol., 2004. **177-178**: p. 747-751.

151. Zolkin, P.I., T.V. Yudina, and I.A. Filatova, *Biocompatible carbon materials.* Perspekt. Mater., 2000: p. 48-53.

152. Davydov, V.A., et al., *Size-Dependent Phase Transition of Diamond to Graphite at High Pressures.* J. Phys. Chem. C, 2007. **111**: p. 12918-12925.

153. Bello, I., et al., *Effects at reactive ion etching of CVD diamond.* Thin Solid Films, 2000. **368**: p. 222-226.

154. Francz, G., P. Oelhafen, and J. Ullmann, *Structural changes in diamond and amorphous carbon induced by low-energy ion irradiation.* Phys. Rev. B: Condens. Matter, 1996. **54**: p. 7067-7073.

155. Gippius, A.A., et al., *Defect engineering in ion-implanted diamond.* Mater. Res. Soc. Symp. Proc., 1998. **510**: p. 431-436.

156. Kalish, R., *Ion-implantation in diamond and diamond films: doping, damage effects and their applications.* Appl. Surf. Sci., 1997. **117/118**: p. 558-569.

157. Kalish, R., et al., *The nature of damage in ion-implanted and annealed diamond.* Nucl. Instrum. Methods Phys. Res., Sect. B, 1999. **148**: p. 626-633.

158. Galkina, T.I., et al., *Bolometric detector embedded in a polycrystalline diamond grown by chemical vapor deposition.* Phys. Solid State, 2007. **49**: p. 654-659.

159. Gippius, A.A., et al., *Formation and characterization of graphitized layers in ion-implanted diamond.* Diamond Relat. Mater., 1999. **8**: p. 1631-1634.

160. Gippius, A.A., et al., *Defect-induced graphitisation in diamond implanted with light ions.* Physica B, 2001. **308-310**: p. 573-576.

161. Gippius, A.A., et al., *Diamond-graphite transformation induced by light ions implantation.* Diamond Relat. Mater., 2003. **12**: p. 538-541.

162. Gonzalez-Hernandez, J., et al., *Graphitization of amorphous diamondlike carbon films by ion bombardment.* J. Vac. Sci. Technol., A, 1988. **6**: p. 1798-802.

163. Hickey, D.P., K.S. Jones, and R.G. Elliman, *Amorphization and graphitization of single-crystal diamond - A transmission electron microscopy study.* Diamond Relat. Mater., 2009. **18**: p. 1353-1359.

164. Kalish, R. and S. Prawer, *Graphitization of diamond by ion impact: Fundamentals and applications.* Nucl. Instrum. Methods Phys. Res., Sect. B, 1995. **106**: p. 492-9.

165. Khmelnitskiy, R.A., et al., *Optical characterization of graphitized layers in ion-implanted diamond.* Proc. SPIE-Int. Soc. Opt. Eng., 1997. **3484**: p. 204-211.

166. Olivero, P., et al., *Direct fabrication of three-dimensional buried conductive channels in single crystal diamond with ion microbeam induced graphitization.* Diamond Relat. Mater., 2009. **18**: p. 870-876.

167. Prins, J.F., *Graphitization and related variable-range-hopping conduction in ion-implanted diamond.* J. Phys. D: Appl. Phys., 2001. **34**: p. 2089-2096.

168. Saada, D., J. Adler, and R. Kalish, *Computer simulation of damage in diamond due to ion impact and its annealing.* Phys. Rev. B: Condens. Matter Mater. Phys., 1999. **59**: p. 6650-6660.

169. Uzan-Saguy, C., et al., *Damage threshold for ion-beam induced graphitization of diamond.* Appl. Phys. Lett., 1995. **67**: p. 1194-6.

170. Zhang, X.K., et al., *Graphitization of diamond films induced by ion implantation.* Phys. Status Solidi A, 1992. **129**: p. K97-K99.

171. Zaitsev, A.M., *Carbon nanowires made on diamond surface by focused ion beam.* Phys. Status Solidi A, 2005. **202**: p. R116-R118.

172. Zaitsev, A.M., A.M. Levine, and S.H. Zaidi, *Carbon nanowire-based temperature sensor.* Phys. Status Solidi A, 2007. **204**: p. 3574-3579.

173. Zaitsev, A.M., A.M. Levine, and S.H. Zaidi, *Temperature and chemical sensors based on FIB-written carbon nanowires.* IEEE Sens. J., 2008. **8**: p. 849-856.

174. Bernard, M., et al., *Electron cyclotron resonance oxygen plasma etching of diamond.* Diamond Relat. Mater., 2004. **13**: p. 287-291.

175. Hwang, D.S., T. Saito, and N. Fujimori, *New etching process for device fabrication using diamond.* Diamond Relat. Mater., 2004. **13**: p. 2207-2210.

176. Kiyohara, S., Y. Yagi, and K. Mori, *Plasma etching of CVD diamond films using an ECR-type oxygen source.* Nanotechnology, 1999. **10**: p. 385-388.

177. Lee, C.L., et al., *Etching and micro-optics fabrication in diamond using chlorine-based inductively-coupled plasma.* Diamond Relat. Mater., 2008. **17**: p. 1292-1296.

178. Masuda, H., et al., *Fabrication of a nanostructured diamond honeycomb film.* Adv. Mater., 2000. **12**: p. 444-447.

179. Pearton, S.J., et al., *ECR plasma etching of chemically vapor deposited diamond thin films.* Electron. Lett., 1992. **28**: p. 822-4.

180. Ramesham, R., et al., *Plasma etching and patterning of CVD diamond at <100° for microelectronics applications.* Thin Solid Films, 1997. **304**: p. 245-251.

181. Seth, J., et al., *Lithographic application of diamond-like carbon films.* Thin Solid Films, 1995. **254**: p. 92-5.

182. Shiomi, H., *Reactive ion etching of diamond in O2 and CF4 plasma, and fabrication of porous diamond for field emitter cathodes.* Jpn. J. Appl. Phys., Part 1, 1997. **36**: p. 7745-7748.

183. Urruchi, W.I., et al., *Etching of DLC films using a low intensity oxygen plasma jet.* Diamond Relat. Mater., 2000. **9**: p. 685-688.

184. Vivensang, C., et al., *Reactive ion etching of diamond and diamond-like carbon films.* Diamond Relat. Mater., 1994. **3**: p. 645-9.

185. Schwan, J., et al., *Raman spectroscopy on amorphous carbon films.* J. Appl. Phys., 1996. **80**: p. 440-447.

186. Tamor, M.A. and W.C. Vassell, *Raman "fingerprinting" of amorphous carbon films.* J. Appl. Phys., 1994. **76**: p. 3823-30.

187. Ambegaokar, V., B.I. Halperin, and J.S. Langer, *Hopping conductivity in disordered systems.* Phys. Rev. B, 1971. **[3]4**: p. 2612-20.

188. Lewis, A., *Evidence for the Mott model of hopping conduction in the anneal stable state of amorphous silicon.* Phys. Rev. Lett., 1972. **29**: p. 1555-8.

189. Massarani, B., J.C. Bourgoin, and R.M. Chrenko, *Hopping conduction in semiconducting diamond.* Phys. Rev. B, 1978. **17**: p. 1758-69.

190. Boudou, J.P., et al., *Oxygen plasma modification of pitch-based isotropic carbon fibres.* Carbon, 2003. **41**: p. 41-56.

191. Bubert, H., et al., *Characterization of the uppermost layer of plasma-treated carbon nanotubes.* Diamond Relat. Mater., 2003. **12**: p. 811-815.

192. Chen, C., et al., *Oxygen Functionalization of Multiwall Carbon Nanotubes by Microwave-Excited Surface-Wave Plasma Treatment.* J. Phys. Chem. C, 2009. **113**: p. 7659-7665.

193. Ji, S., et al., *Research on graphitization of accelerant polishing technique for CVD diamond film.* Adv. Mater. Res., 2010. **102-104**: p. 639-643.

194. Takada, T., et al., *Surface modification and characterization of carbon black with oxygen plasma.* Carbon, 1996. **34**: p. 1087-1091.

195. Tay, B.K., et al., *Study of surface energy of tetrahedral amorphous carbon films modified in various gas plasma.* Diamond Relat. Mater., 2003. **12**: p. 2072-2076.

196. Hutchison, G.R., et al., *Adsorption of Polar Molecules on a Molecular Surface.* J. Phys. Chem. B, 2001. **105**: p. 2881-2884.

197. Fan, Y., M. Burghard, and K. Kern, *Chemical defect decoration of carbon nanotubes.* Adv. Mater., 2002. **14**: p. 130-133.

198. Ferrari, A.C. and J. Robertson, *Interpretation of Raman spectra of disordered and amorphous carbon.* Phys. Rev. B: Condens. Matter Mater. Phys., 2000. **61**: p. 14095-14107.

199. Pimenta, M.A., et al., *Studying disorder in graphite-based systems by Raman spectroscopy.* Phys. Chem. Chem. Phys., 2007. **9**: p. 1276-1291.

200. Hurd, C.M., *Quantum tunnelling and the temperature dependent DC conduction in low-conductivity semiconductors.* J. Phys. C: Solid State Phys., 1985. **18**: p. 6487-99.

201. Colesniuc, C.N., et al., *Exponential behavior of the Ohmic transport in organic films.* Phys. Rev. B: Condens. Matter Mater. Phys., 2011. **83**: p. 085414/1-085414/7.

202. Simmons, J.G., *Intrinsic fields in thin insulating films between dissimilar electrodes.* Phys. Rev. Lett., 1963. **10**: p. 10-12.